

BINARY BLACK HOLES IN DENSE STAR CLUSTERS: EXPLORING THE THEORETICAL UNCERTAINTIES

SOURAV CHATTERJEE, CARL L. RODRIGUEZ, & FREDERIC A. RASIO
Center for Interdisciplinary Exploration & Research in Astrophysics (CIERA)
Physics & Astronomy, Northwestern University, Evanston, IL 60202, USA
sourav.chatterjee@northwestern.edu

Draft version January 30, 2022

ABSTRACT

The exciting discovery of gravitational waves from merging black hole (BH) binaries by Advanced LIGO has generated widespread interest in the astrophysical origin of these sources. Dense star clusters such as globular clusters (GCs) are expected to form large numbers of stellar BHs. However, what happens to these BHs after formation remains somewhat uncertain. Recent theoretical studies with N -body simulations predict that large numbers of stellar BHs could remain bound to at least some GCs at present, and merging BH–BH binaries are produced dynamically in significant numbers. Numerical simulations usually make a “standard” set of assumptions related to, e.g., BH formation in supernovae, stellar winds, binary properties of high-mass stars, and initial stellar mass function (IMF). However, these assumptions have large uncertainties. Here we systematically vary model assumptions within existing uncertainties and study the effects on the evolution of BHs in GCs, and on the final structural properties of GCs. This is made possible by the use of a parallel Monte Carlo code, which provides much higher computational speed than direct N -body codes, thereby allowing large numbers of models to be computed. We find that variations in initial assumptions can set otherwise identical initial clusters on completely different evolutionary paths, significantly affecting their observable properties at present, or even affecting the cluster’s very survival to the present. However, these changes usually do not affect the numbers or properties of merging BH–BH binaries produced by GCs. The only exception is that varying assumptions about stellar IMF and winds can significantly change the masses of BHs in merging binaries. For a given IMF and metallicity, all other variations (e.g., in initial binary properties and binary fraction) leave the numbers and masses of BH–BH mergers largely unchanged. This is in contrast to binary population synthesis models for the field, where results are very sensitive to a large number of uncertain parameters in the initial properties of binaries and in the binary stellar evolution physics. We discuss our results in the context of the recently detected BH–BH merger GW150914, assuming that it originated in a GC. The very large BH masses in this system are likely not common, even with weak winds and low metallicity; instead, the properties inferred for the other LIGO trigger event, LVT151012, are closer to what we would predict for the bulk of BH–BH mergers produced dynamically in GCs.

Subject headings: black hole physics—methods: numerical—methods: statistical—stars: black holes—stars: kinematics and dynamics—globular clusters: general

1. INTRODUCTION

Our understanding of how black holes (BHs) evolve inside star clusters has a long and varied history. Following the classic work by Spitzer (1969), it was suggested that old (~ 12 Gyr) globular clusters (GCs) cannot retain a significant BH population up to the present day. It was argued that, due to the much higher mass of the BHs compared to typical stars, the BHs will quickly ($\lesssim 10^2$ Myr) mass segregate to form an isolated subcluster that is dynamically decoupled from the GC. Due to the small size, high density, and small number of objects in the subclusters, relaxation and strong encounters were expected to eject the majority of BHs on a timescale ~ 1 Gyr. Thus, at most a few BHs would remain in the old GCs observed in the Milky Way (MW, e.g., Kulkarni et al. 1993; Sigurdsson & Hernquist 1993; Portegies Zwart & McMillan 2000; Kalogera et al. 2004). Furthermore, it was argued that if significant numbers of BHs are present in today’s GCs, a subset of them might be in accreting binary systems, and detectable as X-ray sources. However, observations of luminous X-ray sources in the

MW GCs prior to 2012 suggested that *all* of these sources are accreting neutron stars and not BHs, consistent with theoretical expectation at the time (e.g., van Zyl et al. 2004; Lewin & van der Klis 2006; Altamirano et al. 2010, 2012; Bozzo et al. 2011).

This classical picture started to change with recent discoveries of BH candidates in extragalactic GCs, characterized by their super-Eddington luminosities and high variability on short timescales (MacCarone et al. 2007; Irwin et al. 2010). More recently, with the completion of the upgraded VLA, surveys combining radio and X-ray data for the MW GCs detected quiescent BHs by comparing their radio and X-ray luminosities (e.g., Strader et al. 2012; Chomiuk et al. 2013). Interestingly, the MW GCs containing the detected BH candidates show large ranges in structural properties, indicating that the retention of BHs may be quite common. Several recent or ongoing surveys promise much richer observational constraints on this question (e.g., Strader et al. 2013; Strader 2014; Miller-Jones et al. 2014a,b).

To be detectable either via electromagnetic signatures

or via gravitational waves (GW) from BH–BH mergers, the BHs must be in binary systems with very specific ranges of properties. Although dynamical interaction can enhance the production of binaries containing a BH (BBHs) (e.g., Kundu et al. 2002; Pooley et al. 2003), modern simulations find that the fraction of BHs in binaries is typically low (e.g., Morscher et al. 2015). Hence, it has been argued that detection of just a few BH candidates in GCs indicates the existence of a much larger population of BHs that are not detectable (e.g., Strader et al. 2012; Umbreit 2012; Morscher et al. 2013, 2015). Indeed, recent numerical studies have found that BH ejection is not nearly as efficient as was previously thought. In these studies, it has been shown that the BH subcluster does not stay decoupled from the rest of the cluster for prolonged periods. The same interactions that eject BHs from the subcluster also cause it to expand and re-couple with the rest of the cluster, dramatically increasing the timescale for BH evaporation (e.g., Breen & Heggie 2013; Morscher et al. 2015). These simulations suggest that tens to thousands of BHs may remain in today’s GCs (e.g., Mackey et al. 2008; Moody & Sigurdsson 2009; Aarseth 2012; Morscher et al. 2013, 2015).

Most recently, Morscher et al. (2015) showed that the presence of a significant number of BHs can dramatically alter the overall dynamical evolution of GCs. Through repeated cycles of core-collapse and core re-expansion, BH-dynamics acts as a significant and persistent source of energy. On the other hand, the clustered environment and high frequency of strong scattering interactions, especially involving binaries, can change the numbers and properties of BBHs that form inside clusters (e.g., Rodriguez et al. 2015, 2016a; Antonini et al. 2016). Both of these aspects intricately depend on several physical processes, many of which lack strong observational constraints. For example, the distribution of the natal kicks the BHs receive can control how many of them will be directly ejected from the GCs immediately upon formation. Natal kicks also control the fraction of BHs that may retain their binary companions after SN. The high end of the stellar initial-mass function (IMF) determines how many BHs a cluster can form. The binary fraction and binary orbital properties can alter the binary stellar evolution of a BBH (or their progenitors) as well as the rate at which they take part in dynamical encounters. In addition, the ratio between the BH mass and the average stellar mass, also directly determined by the IMF, determines the timescale for BHs to sink to the center. Answers to a wide variety of questions, such as how many BHs and BBHs can a GC retain at present, how many BBHs it can form over its whole lifetime, at what rate do BHs and BBHs get ejected from the clusters, and how do the BHs affect the overall evolution of the clusters, can potentially depend on these initial assumptions. Hence, we must understand the sensitivity of our models to initial conditions and assumptions that are poorly constrained by existing observations.

In this study, we vary the initial assumptions regarding the high-mass stars and BHs that are usually considered “standard” in theoretical studies of clusters. In particular, we vary the stellar IMF, the birth-kick distribution for the BHs, and the primordial binary fraction and the binary properties for massive stars. We also vary the assumed prescription for mass loss via stellar winds. Start-

ing from otherwise identical initial star clusters, we study how varying these assumptions affect BH populations, and the overall evolution and final observable properties of the host clusters. We also study how these initial assumptions affect the number and properties of merging BH–BH binaries. We put these findings in the context of the recent landmark detection of GWs from a BH–BH merger by Advanced LIGO (Abbott et al. 2016a,b).

In §2 we describe our numerical models and we list the initial assumptions that we vary. In §4 we show how the various assumptions affect the overall evolution and final observable properties of star clusters. §5 focuses on how these assumptions and resulting differences in the cluster evolution as a whole alter the binary properties of BHs. In §6 we focus on the numbers and properties of BH–BH mergers and put those results in the context of the recent discovery of GW150914 (Abbott et al. 2016a). We summarize our results and conclude in §7.

2. NUMERICAL MODELS

We use our Hénon-type (Hénon 1971) Cluster Monte Carlo (CMC) code, developed and rigorously tested in our group over the past 15 years (Joshi et al. 2000, 2001; Fregeau et al. 2003; Umbreit et al. 2012; Pattabiraman et al. 2013; Chatterjee et al. 2010, 2013a,b). For a detailed description of the most recent updates and parallelization see Pattabiraman et al. (2013) and Morscher et al. (2015). The Monte Carlo approach is more approximate than a direct N -body integration (e.g., Aarseth 2010), but requires only a fraction of the computational time. This rapidity allows us to fully explore the parameter space of dense star clusters. Results from CMC have been extensively compared to recent state-of-the-art N -body simulations, and were found to produce excellent agreement in all quantities of interest in this study (Rodriguez et al. 2016b).

2.1. Standard Assumptions

In order to understand the influence of each initial assumption on the production and subsequent evolution of BHs in a cluster, we anchor our numerical models using the same assumptions as used in Morscher et al. (2015). We call this our “standard” model and denote it as **S** (Table 1). Our standard model initially has $N = 8 \times 10^5$ stars. The position and velocities of the stars are set according to a King profile with $W_0 = 5$ (King 1962, 1965, 1966). We adopt the commonly-used IMF presented in Kroupa (2001), and use the central value for each slope in the different mass ranges between $0.1\text{--}100 M_\odot$ to assign masses to these stars. In model **S** we assume an initial binary fraction $f_b = 0.05$. This is realized by randomly selecting the appropriate number ($N_b = N \times f_b$) of stars, independent of their masses or positions in the cluster, and assigning binary companions to them. The mass of the secondary (m_s) is drawn from a uniform distribution with a lower limit taken from the assumed IMF, $m_{\min} = 0.1 M_\odot$, and an upper limit equal to the mass of the primary (m_p). The orbital period (P) is drawn from a distribution flat in $\log P$ between 5 times the sum of the radii for the binary companions, and the local hard–soft boundary given by $v_{\text{orb}} = v_\sigma$, where, v_{orb} is the orbital velocity and v_σ is the local velocity dispersion. Note that, although all initial binaries are locally hard, dynamical evolution can make them soft at a later

time, either by increasing the local velocity dispersion of other stars (typically in the core) or by moving the binary from its initial location to where the velocity dispersion is higher (due to mass segregation). Such soft binaries are maintained in all our simulations until strong scattering encounters disrupt them. The initial orbital eccentricities for the binaries are drawn from a thermal distribution.

Single and binary stellar evolution is performed with SSE and BSE (Hurley et al. 2000, 2002). We have modified the prescription for stellar remnant formation in SSE and BSE by using the results of Fryer & Kalogera (2001) and Belczynski et al. (2002). All core-collapsed neutron stars get birth kicks drawn from a Maxwellian distribution with $\sigma = \sigma_{\text{NS}} = 265 \text{ km s}^{-1}$. We assume momentum ($|\vec{p}|$) conserving kicks for BHs following the prescription of Belczynski et al. (2002). BHs formed via the direct collapse scenario do not get any natal kicks, since there is no associated explosion or mass loss. BHs formed with significant fallback get natal kicks calculated by initially sampling from the same kick distribution as the neutron stars, but reduced in magnitude according to the fractional mass of the fallback (x_{fb}) material (see Morscher et al. 2015, for a more detailed description of our standard model S).

Below we describe how we vary the above-mentioned initial assumptions. In each case we describe only the assumptions we change relative to the baseline model S, with all other initial conditions held constant.

2.2. Initial Binary Fraction and Binary Properties of Massive Stars

One source of uncertainty in setting up the initial conditions is whether the binary fraction depends on the stellar mass. We create two models, F0 and F1, varying the fraction of high-mass stars ($> 15 M_{\odot}$) that are initially in binaries ($f_{b,\text{high}}$). In models F0 and F1, we adopt limiting initial values of $f_{b,\text{high}} = 0$ and 1, respectively (Table 1). We assign the binaries in these two models such that the overall binary fraction f_b is kept fixed at 0.05. In model F0, $N_b = 0.05 \times N$ stars are randomly chosen from all stars with mass $\leq 15 M_{\odot}$ and are assigned as binaries. In model F1, we first assign all stars with mass $> 15 M_{\odot}$ as binaries. We randomly choose the appropriate residual number of low-mass stars ($\leq 15 M_{\odot}$) and assign them as binaries to make $f_b = 0.05$. In F0 and F1, the distributions for the mass ratios (q) and the orbital properties are identical to model S.

In addition to the binary fraction in high-mass stars, the binary orbital properties can potentially affect both the formation and interaction rate of BHs in a cluster. The observed distributions of initial separations and q for binaries may have significant uncertainties and selection biases. To understand the effects of these initial assumptions, we create a set of models where we vary the initial binary properties of the high-mass ($> 15 M_{\odot}$) stars. In these models, we assume that the initial $f_{b,\text{high}} = 0.7$ following the observational constraint provided in Sana et al. (2012). In addition, we choose an initial period distribution described by $dn/d \log P \propto P^{-0.55}$ for the high-mass stars (Sana et al. 2012). The number of binaries for low-mass stars are again adjusted so that the overall f_b is ≈ 0.05 , similar to model S. We denote these models with “F0.7.” Within this variant, we also con-

sider two different q distributions for the high-mass binaries. In one, we use a uniform distribution of q between $q = m_{\text{min}}/m_p$ and 1. These models are denoted with the string “Ms0.1”. Another set of models uses the same uniform distribution in q , but within a much smaller range, 0.6 and 1. We denote this set of models with the string “q0.6” (Table 1).

2.3. Natal Kick Distribution for Black Holes

It has been widely accepted that the neutron stars get large natal kicks when they form via core-collapse SN (e.g., Cordes et al. 1993; Lyne & Lorimer 1994; Wang et al. 2006; Zuo 2015). However, the magnitudes of natal kicks imparted to BHs, is still a matter of debate. Observational constraints come from modeling the kicks required to explain the positions and velocities of known BH X-ray binaries (XRB) in the MW galactic potential. Detailed analysis of individual BH XRBs results in widely varying constraints on their natal kick magnitudes (e.g., Brandt et al. 1995; Nelemans et al. 1999; Willems et al. 2005; Gualandris et al. 2005; Dhawan et al. 2007; Fragos et al. 2009; Wong et al. 2012, 2014). Instead of modeling individual systems, Repetto et al. (2012) and Repetto & Nelemans (2015) have performed population synthesis using different assumptions of natal kick distributions and compared their results with the positions of the observed BHs in the MW. They have found that BHs may get large kicks, perhaps even as large as the neutron stars formed via core-collapse SN. In addition, they have not found evidence of a mass-dependent kick distribution, which would be expected for the widely used $|\vec{p}|$ -conserving kick prescription. Recent theoretical study of core-collapse SN by Pejcha & Thompson (2015) also suggests that the birth kicks may not be directly correlated with the BH mass. In short, the distribution of formation kicks for BHs is largely uncertain, even at the qualitative level.

In addition to the one used in S, we create models with three different natal kick distributions for the BHs. These models assume that the kick magnitudes are independent of the BH masses and x_{fb} , and are drawn from a Maxwellian given by $\sigma = \sigma_{\text{BH}}$. We adopt three variations that are obtained by using $\sigma_{\text{BH}} = \sigma_{\text{NS}} = 265 \text{ km s}^{-1}$ (denoted by the string “K1”), $\sigma_{\text{BH}} = 0.1\sigma_{\text{NS}}$ (denoted by the string “K2”), and $\sigma_{\text{BH}} = 0.01\sigma_{\text{NS}}$ (denoted by the string “K3”) in Table 1.

2.4. Initial Stellar Mass Function

A lot of observational effort is aimed towards finding the expected IMF for stars born in clusters (e.g., Kroupa & Boily 2002, and the references therein). Of course, the number of BHs a cluster can form is directly dependent on the number of massive BH-progenitor stars it initially contains. This, in turn, is directly dependent on the stellar IMF, especially the power-law slope of the IMF near the high-end of stellar masses. As described earlier, our standard models use the central values for the IMF slopes from Kroupa (2001). However, we note that the best-fit power-law exponents α in $dn/dm \propto m^{-\alpha}$ throughout all mass ranges have large uncertainties. For example, the power-law exponent α_1 , for stars more massive than $1 M_{\odot}$ is 2.3 with 1σ error of 0.7 (Kroupa 2001). We vary α_1 within the quoted 1σ uncertainties, and create mod-

els with $\alpha_1 = 1.6$ (denoted using the string “If”) and $\alpha_1 = 3$ (denoted using the string “Is”) in Table 1.

2.5. Stellar Wind Prescription

The details of how stars lose mass to stellar winds is complicated and hard to model theoretically. Most stellar evolution prescriptions instead model the mass and metallicity-dependent stellar winds by calibrating the wind-driven mass loss to catalogues of observed stars (e.g., de Boer et al. 1997; Van Eck et al. 1998; Hurley et al. 2000; Vink et al. 2001). The assumed wind prescription dramatically affects the mass of the BH progenitor at the time of SN, which in turn determines the mass of the resultant BH. The wind prescription described in Hurley et al. (2000) is widely used as part of the SSE and BSE software packages in many widely-used cluster dynamics codes. The majority of our models use this stellar wind prescription. For simplicity, we call BSE’s implementation for winds as the “strong wind” prescription.

Recent observations of high-mass stars suggest that the stellar winds may not be as strong as suggested by earlier studies (e.g., Vink et al. 2001; Vink 2008; Belczynski et al. 2010a,b; Dominik et al. 2012; Spera et al. 2015). The details of this wind prescription, based on, e.g., Vink et al. (2001) is documented in detail in Belczynski et al. (2010b), and implemented in our code in (Rodriguez et al. 2016a). For simplicity, we call this implementation the “weak wind” prescription. All models adopting weak winds are denoted with the string “W” in Table 1.

2.6. Other Assumptions

In addition to the above variations to our standard model S, we also vary the galactocentric distance (r_G), metallicity (Z), the initial virial radius (r_v), and the overall spread in the stellar IMF for a handful of models. The details of all models and initial assumptions are listed in Table 1.

3. DERIVATION OF OBSERVED CLUSTER PROPERTIES

The definitions for key structural properties in numerical models are often different from those defined by observers for real clusters (e.g., Chatterjee et al. 2013b). To be consistent, we “observe” our simulated models to extract structural properties with definitions similar to those used for real observations. We use the last snapshot from all our model clusters to extract the observable structural properties. All relevant final structural properties, measured both using theoretical definitions, and observers’ definitions are listed in Table 2.

3.1. Estimation of “Observed” Structural Properties

We create two-dimensional projections for each model assuming spherical symmetry. The half-light radius, $r_{hl,obs}$, is then estimated by finding the projected radius containing half of the total light. We obtain the observed core radius, $r_{c,obs}$, and the observed central density, $\Sigma_{c,obs}$, by fitting an analytic King model to the cumulative stellar luminosity at a given projected radius including stars within a projected distance of $r_{hl,obs}$ from the center (King 1962, their Eq. 18). This method was suggested earlier by Morscher et al. (2015). Since,

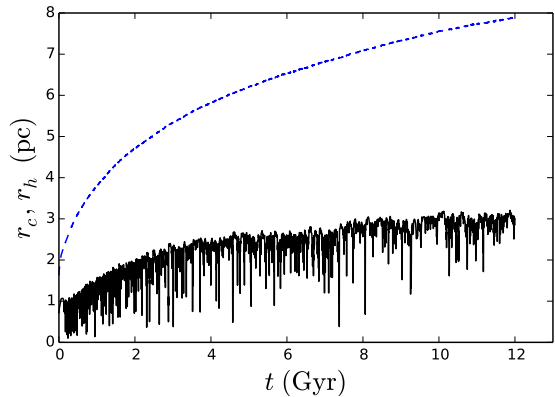


FIG. 1.— Evolution of the core radius (r_c) and the half-mass radius (r_h) for model S. The solid (black) and dashed (blue) lines denote r_c and r_h , respectively. The spikes in r_c due to BH-driven core collapse continue until the end of the simulation at 12 Gyr. Both r_c and r_h expand all the way to the end.

this approach avoids binning of data, this is more robust against statistical fluctuations, especially at low projected distances compared to the often-used method of fitting the King profile directly to the surface brightness profile (SBP).

We estimate the observed central velocity dispersion $v_{\sigma,c,obs}$ by taking the standard deviation of the magnitudes of the three-dimensional velocities of all luminous stars (excluding compact objects) within a projected distance of $r_{c,obs}$. In case of binaries, we take into account the center of mass velocities.

3.2. Estimation of Dissolution Times

Depending on initial assumptions, some of our cluster models get tidally disrupted before the integration stopping time of 12 Gyr. The basic assumptions of our Monte Carlo approach are spherical symmetry, and a sufficiently large N to ensure that the relaxation timescale is significantly longer than the dynamical timescale. Both assumptions break down for clusters that have begun to tidally disrupt, since the tidal boundary is not spherically symmetric, and a disrupting cluster can lose mass on a timescale \ll than the relaxation time. To that end, once $t_r(t) > M(t)/\dot{M}$ for a cluster, where t_r , and M denote relaxation time and total cluster mass respectively, we consider the cluster to have dissolved. For clusters that dissolve before 12 Gyr, we list the approximate dissolution times and mark them as “Dissolved” in Table 2.

4. OVERALL CLUSTER EVOLUTION

Fig. 1 shows the evolution of the core radius (r_c) and the half-mass radius (r_h) for our standard model S. As expected, r_c shows repeated downward spikes indicating collapse of the BH subcluster (e.g., Morscher et al. 2015). Dynamical ejections and binary formation following each BH-driven core collapse produces energy, reversing the collapse and re-expanding the BH positions to mix with the rest of the cluster. Through repeated collapses, the overall r_c increases until the integration is stopped at 12 Gyr, and attains $r_c = 2.8 \pm 0.1$ pc. The error-bar here denotes the 1σ fluctuations during the last 1 Myr of the cluster’s evolution. r_h monotonically increases as well, attaining a final value of about 8 pc.

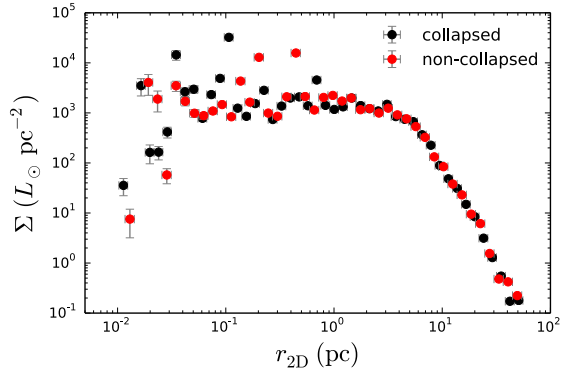


FIG. 2.— Comparison between the SBPs at two different times, one corresponding to a core-collapsed state, seen as the downward spikes in Fig. 1 (at $t = 9.27$ Gyr; black), and the other corresponding to a non-collapsed state (at $t = 9.29$ Gyr; red) for model S. The theoretically defined core radius changes from $r_c \approx 0.4$ during the collapsed state to about 3 pc out of that collapse. However, the observable SBP barely changes.

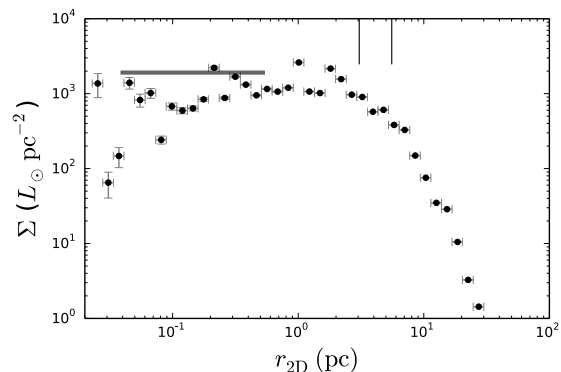


FIG. 3.— Final SBP at $t = 12$ Gyr for model S. The dots denote the surface luminosity density. While calculating the SBP, we discard stars brighter than $20 L_\odot$ to reduce noise from a small number of bright giant stars (e.g., Noyola & Gebhardt 2006). The horizontal line denotes the central surface luminosity density ($\Sigma_{c,obs}$) based on the best-fit King model (§3). The vertical lines denote the observed core radius $r_{c,obs}$ (obtained from the King fit) and observed half-light radius $r_{hl,obs}$.

Of course, an astronomer observing this cluster would measure different values for the structural quantities. Since the core collapse at any time during the evolution involves only a small number of the most massive BHs in the cluster, the observable SBP is insensitive to these collapses. For example, Fig. 2 shows the SBPs for the same model cluster at two different times during its evolution, one when the cluster is in a core-collapsed state and the other when the cluster is out of it. There is no difference between the SBPs, although the theoretical r_c changes from about 0.4 to 2.8 pc, between the collapsed and non-collapsed states. Thus, the core collapses driven by BH dynamics in these clusters are not observable.

Fig. 3 shows the SBP including stars with luminosity $L_* \leq 20 L_\odot$ for model S at $t = 12$ Gyr. At this time model S has $\Sigma_{c,obs} \approx 2.7 \times 10^3 L_\odot \text{pc}^{-2}$, $r_{hl,obs} = 5.5$ pc, and $r_{c,obs} = 3$ pc. Hence, to an observer S would appear as a cluster with low central density and puffed-up core.

In general, if a large number of BHs remain bound to the host cluster, dynamics involving BHs (dynamical for-

mation of new binaries, binary–single and binary–binary scattering, and dynamical ejections from the cluster core) acts as the dominant source of energy in the core. The cluster can start the relaxation-driven core-contraction phase only after this source of energy is sufficiently depleted. The larger the number of retained BHs (N_{BH}) at a given time, the bigger the $r_{c,obs}$ and $r_{c,obs}/r_{hl,obs}$ for the host cluster (Fig. 4). For example, excluding the disrupted clusters, the correlation coefficient between N_{BH} and $r_{c,obs}$ at $t = 12$ Gyr is 0.82 and that between $r_{c,obs}/r_{hl,obs}$ is 0.78. Because of the large amount of energy BH-driven dynamics can inject into the clusters, the central density, $\Sigma_{c,obs}$, also depends strongly on N_{BH} ; $\Sigma_{c,obs}$ and N_{BH} are anti-correlated with a correlation coefficient of -0.3 (Fig. 5).

Note that due simply to the differences in the initial assumptions affecting the high-mass stars, clusters with very similar initial conditions attain widely varying final properties spanning ~ 4 orders of magnitude in N_{BH} , $\gtrsim 2$ orders of magnitude in $r_{c,obs}$, and $\gtrsim 4$ orders of magnitude in $\Sigma_{c,obs}$ at $t = 12$ Gyr (§2; Tables 1 & 2).

We find that the most dramatic differences in the overall final properties of a star cluster come from the differences in N_{BH} . The variations in initial assumptions can change the evolution of N_{BH} in different ways, and as a result, change the overall evolution of the cluster and its structural properties (e.g. $r_{c,obs}$, $r_{hl,obs}$, and $\Sigma_{c,obs}$). We find that the most important assumption that determines the evolution of N_{BH} in a cluster is the natal kick distribution for the BHs. Hence, we start by discussing the effects of initial assumptions related to BH-formation kicks.

4.1. Effects of the Natal Kick Distribution for BHs

The assumed natal kick distribution for BHs directly controls N_{BH} at a given time, and through that it controls the evolution of the cluster. For example, Fig. 6 shows the evolution of N_{BH} , r_c , r_h , r_c/r_h , and the final SBPs for four identical models, all at a fixed $r_G = 8$ kpc. These models vary only in the assumed distribution of natal kicks for the BHs. We find that if the BHs are given full NS kicks, i.e., $\sigma_{BH} = \sigma_{NS}$, most of the BHs are ejected from the cluster within $t \approx 20$ Myr, immediately after formation. Without the source of energy from BH dynamics at the center, the cluster starts contracting due to two-body relaxation after the initial expansion from mass loss via stellar evolution. At about 11 Gyr the cluster reaches the so-called binary-burning phase, when core-contraction is arrested due to extraction of binding energy from binary orbits via super-elastic scattering encounters (e.g., Heggie & Hut 2003). Based on the final SBP, this cluster would appear as a high-density core-collapsed cluster (Fig. 6; see also Chatterjee et al. 2013b). In contrast, clusters modeled with other natal kick distributions, where the BHs essentially receive much lower kicks compared to the neutron stars formed via core-collapse SN, do retain large numbers of BHs all the way through 12 Gyr. Due to the energy produced from BH dynamics, each of these clusters continues to expand till the end. K2 with $\sigma_{BH} = 0.1\sigma_{NS}$ contains about 200 BHs at $t = 12$ Gyr, a sufficient number to keep the cluster in an expanded state. However, the rate of expansion is lower compared to models S and K3 where at 12 Gyr, N_{BH} are much higher, with values 464 and 759,

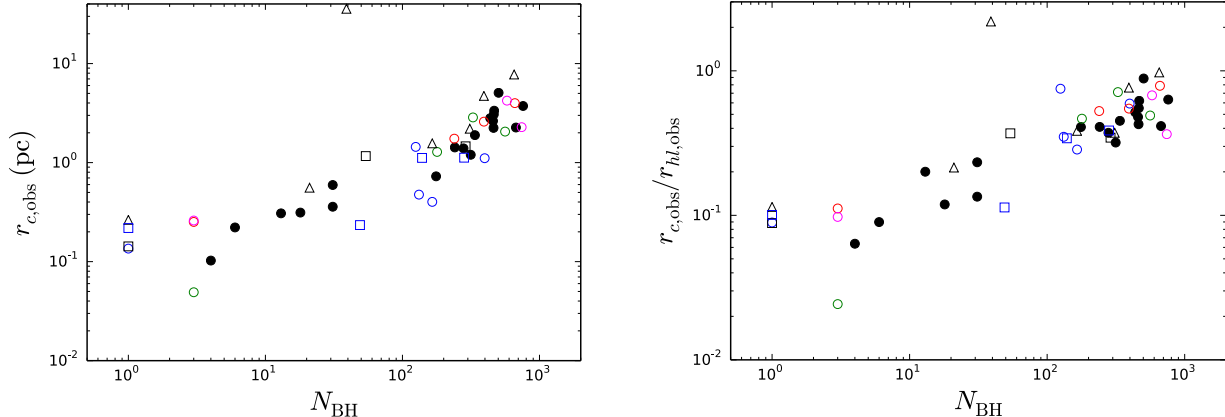


FIG. 4.— Final number of BHs bound to the cluster, N_{BH} vs $r_{c,\text{obs}}$ (Left) and $r_{c,\text{obs}}/r_{\text{hl,obs}}$ (Right) for all models that survived for at least 11 Gyr. Filled black circles represent models with $r_{\text{G}} = 8$ kpc, $r_{\text{v}} = 2$ pc and strong winds. Blue, green, red, and magenta empty circles denote models with the same assumptions for r_{v} and stellar wind, but with $r_{\text{G}} = 1, 2, 4,$ and 20 kpc, respectively. Black triangles denote models with $r_{\text{G}} = 8$ kpc, $r_{\text{v}} = 2$ pc, and weak winds. Black and blue squares both denote models with $r_{\text{G}} = 8$ kpc, $r_{\text{v}} = 1$ pc, and a wider IMF, but with weak and strong winds, respectively. In general, the larger the N_{BH} , the higher the $r_{c,\text{obs}}$ and $r_{c,\text{obs}}/r_{\text{hl,obs}}$. Effects of all other initial assumptions are minor (Table 1). One model is a clear outlier with a very large $r_{c,\text{obs}}$ and moderate N_{BH} : this is model WfK1 (Table 2), which is on the verge of dissolution.

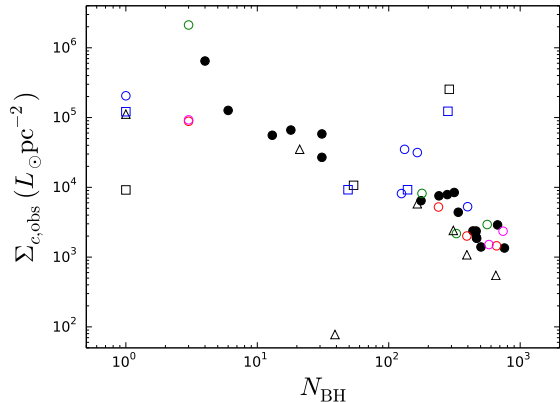


FIG. 5.— N_{BH} vs $\Sigma_{c,\text{obs}}$ for all models that survive for at least 11 Gyr. Point styles are the same as in Fig. 4. The final $\Sigma_{c,\text{obs}}$ is strongly dependent on N_{BH} . Effects of r_{v} , r_{G} , $f_{b,\text{high}}$ and winds are minor, only affecting $\Sigma_{c,\text{obs}}$ through N_{BH} that are bound in the clusters at 12 Gyr. Model WfK1 is on the verge of dissolution and exhibits very low density and moderate N_{BH} .

respectively. While near the end there are indications that the model cluster K2 would start contracting after it ejects some more BHs, models S and K3 are still expanding at $t = 12$ Gyr, and appear as puffy, low-density clusters from their final SBPs. The same initial cluster can evolve to a final observational state with $r_{c,\text{obs}}$ and $\Sigma_{c,\text{obs}}$ varying by orders of magnitude, simply because of changes in the assumed natal kick distribution for its BHs (Table 2).

The significant number of retained BHs can also expand the cluster closer to its tidal radius, making the cluster more prone to disruption from Galactic tides. For example, with otherwise the exact same properties, at $r_{\text{G}} = 1$ kpc, clusters with relatively larger N_{BH} expand more (e.g. SR1Z and K3R1Z), and dissolve much earlier than 12 Gyr. On the other hand, with the same initial conditions, model clusters with relatively lower N_{BH} are safe from tidal disruption even at $r_{\text{G}} = 1$ kpc (e.g., K1R1, K2R1).

In general, the larger the value of N_{BH} , the lower the

final total mass of the cluster. This is because more compact clusters lose less mass via tidal stripping from their host galaxies. The exact amount of expansion, mass loss, and the final cluster mass also depends on the metallicity (Z) of the cluster, since the metallicity controls the wind-driven mass loss and the resulting mass of the BH population. Higher Z leads to the formation of lower-mass BHs, and as a result the overall expansion due to BH ejections is reduced. The adopted wind prescription yields a similar effect. The weak-wind prescription leads to a much lower wind-driven mass loss compared to the strong-wind prescription. As a result, our models with weak winds form massive BHs with higher masses, and eventually undergo more cluster expansion than the models with strong winds. This increased rate of expansion leads to an increased rate of star loss in models with weak winds compared to those with strong winds and is reflected in the final N in these clusters (Table 2).

4.2. Effects of the Assumed IMF

While for a given IMF the BH natal kick distribution is the dominant factor controlling BH retention and overall star cluster evolution, any change to the IMF, especially for the high-mass stars, can also bring about dramatic differences in how the cluster evolves. By directly controlling both the number of high-mass stars (and hence the number of BHs) formed in a cluster, and the average stellar mass, variations in IMF can control the evolution of a cluster and even its survival (Chernoff & Weinberg 1990).

For example, we have tested the effects of variation in the slope α_1 of the IMF for stars more massive than $1 M_{\odot}$ within the quoted uncertainty 2.3 ± 0.7 in Kroupa (2001). Clusters evolve very differently depending on the choice of α_1 (Fig. 7). We first focus on our standard set of models (models S, Is, and If; Table 1). While models with $\alpha_1 = 2.3$ and 3.0 evolve normally and survive until $t = 12$ Gyr, the model with $\alpha_1 = 1.6$ dissolves at around 2 Gyr (see §3.2 for how dissolution times are estimated). At first, mass is lost primarily via stellar winds. Cluster model If loses slightly more mass compared to the other

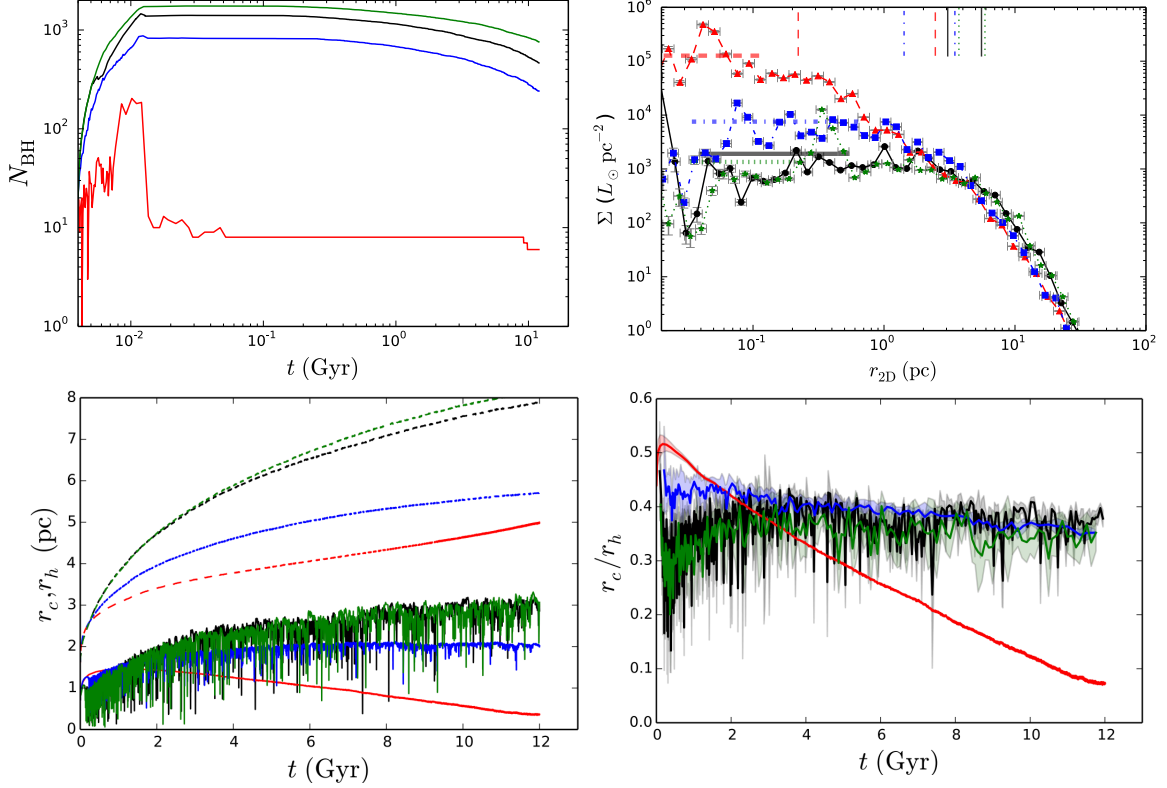


FIG. 6.— Comparison between model clusters S (black), K1 (red), K2 (blue), and K3 (green) (Tables 1, 2) identical except the assumption for the kick distribution during BH-formation. *Top-Left*: Evolution of the bound N_{BH} for the four models. *Bottom-Left*: Evolution of r_c and r_h . Solid and dashed lines denote r_c and r_h , respectively. To reduce scatter we take running averages for r_c/r_h . The lines denote the mean and the shaded regions show 1σ spread. *Top-Right*: Final SBPs for the four models. The horizontal and vertical lines denote $\Sigma_{c,\text{obs}}$, $r_{c,\text{obs}}$, and $r_{hl,\text{obs}}$ for each model. Clearly, the bound N_{BH} depends very strongly on the assumed distribution of formation kicks for the BHs. As a result, the overall evolution of the cluster also alters dramatically. For example, K1 with $\sigma_{\text{BH}} = \sigma_{\text{NS}}$ have only a handful of retained BHs. This cluster evolves to become a dense compact cluster and reaches the binary-burning phase near $t = 12$ Gyr, with a SBP typical of the so-called core-collapsed observed GCs. In contrast, all other models that retain significantly larger numbers of BHs at $t = 12$ Gyr, evolve very differently. S and K3 keep expanding until $t = 12$ Gyr, whereas model K2 ceases to expand at around $t = 8$ Gyr.

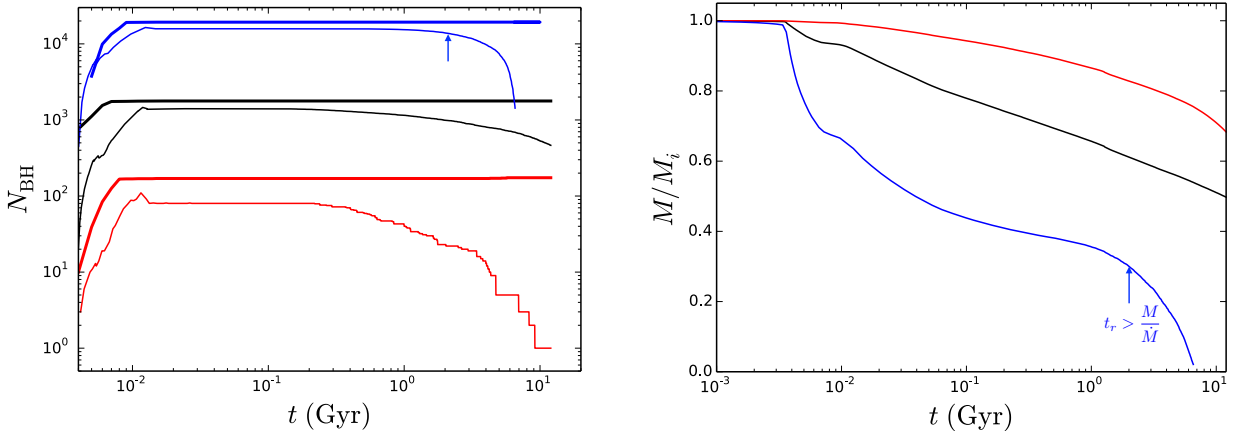


FIG. 7.— Comparison between models with varying IMFs. Each model has a different α_1 , where $\frac{dn}{dm_*} \propto m_*^{-\alpha_1}$ for $m_* > 1 M_\odot$. Black (model S), red (model Is) and blue (model If) lines denote $\alpha_1 = 2.3, 3$, and 1.6 , respectively (see §2; Kroupa 2001). *Left*: Evolution of the total number of BHs formed (thick lines) and total number of BHs retained by the cluster (thin lines). *Right*: Evolution of the cluster mass normalized to the initial cluster mass. Starting from otherwise identical initial conditions, the three clusters meet with very different fates. The cluster model with $\alpha_1 = 1.6$ produces many more BHs compared to other models, expands enormously, and gets disrupted around $t = 2$ Gyr. The approximate disruption time (§3.2) is marked by arrows.

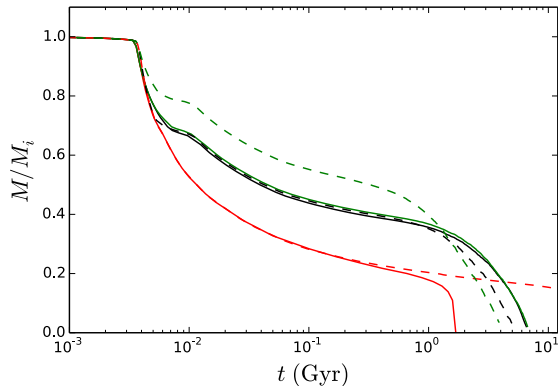


FIG. 8.— Evolution of the star cluster mass normalized by the initial mass of the cluster for models with $\alpha_1 = -1.6$. Black, red, and green lines denote models with our standard kick prescription (models If, WIf), and fallback-independent kick prescriptions with $\sigma_{\text{BH}} = 1$ (models IfK1, WIfK1), and $0.01\sigma_{\text{NS}}$ (models IfK3, WIfK3), respectively. Solid and dashed lines denote models with strong and weak winds, respectively. All of these clusters get disrupted before $t = 12$ Gyr. Models that retain significant numbers of retained BHs, weak winds lead to earlier dissolution of the cluster relative to strong winds. Weak winds lead to formation of higher-mass BHs, which lead to faster expansion of the clusters, and correspondingly higher tidal mass loss compared to the strong wind case. For models with $\sigma_{\text{BH}} = \sigma_{\text{NS}}$, this is reversed, since in this case with very low values of N_{BH} , mass loss from stellar evolution and compact object formation is the dominant effect.

model clusters with steeper α_1 . Dramatic differences appear during the stage when the clusters lose mass via compact object formation. As expected, the steeper the high-end of the IMF, the lower the mass loss from compact object formation. This episode of quick mass loss ends by the time all the BHs are formed and many of the BHs are ejected due to their birth kicks. Following this episode, mass loss slows down and is driven by dynamically BH ejections from the core and mass loss through the tidal boundary. At this stage, the number of retained BHs in a cluster becomes very important. Larger values of N_{BH} lead to more dynamical ejections, which in turn lead to faster cluster expansion and higher tidal mass loss rate. Eventually, if the cluster expands too much, it gets disrupted.

The details of this process depends both on the kick distribution for the BHs as well as the wind-driven mass loss (Fig. 8). During the initial stages, clusters modeled with weak winds lose less mass than those modeled with strong winds. However, lower wind-driven mass loss leads to the formation of more massive BHs. These higher-mass BHs segregate more rapidly in the cluster potential. In addition, higher-mass BHs inject more energy into the cluster via dynamics and ejections than their lower-mass counterparts. As a result, once the cluster is sufficiently old for BH-dynamics to dominate energy production, the clusters modeled with weak winds expand faster and get disrupted earlier than those modeled with strong winds. The higher the number of retained BHs, the bigger the difference between the clusters modeled with strong and weak winds (Fig. 8). This trend is reversed in the models IfK1 and WIfK1, both modeled with the highest natal kicks for the BHs we consider (Table 1). Since in these models almost all BHs are ejected during formation, the above-mentioned difference due to BH-dynamics is not relevant. Instead, since in the high-

kick case, the weak-wind model loses less mass than the strong-wind model, IfK1 is disrupted earlier than WIfK1.

4.3. Effects of Other Assumptions

The process and timescale for energy production from BH dynamics depend critically on the mass segregation timescale (t_S) in a cluster (e.g., Breen & Heggie 2013; Morscher et al. 2013, 2015). The mass segregation timescale of a massive object depends on the relaxation timescale (t_r), and the ratio of its mass to the average stellar mass ($\langle m \rangle$) in its neighborhood, $t_S \propto t_r \frac{\langle m \rangle}{m_i}$ (e.g., Gürkan et al. 2004). Thus, N_{BH} and as a result, the overall cluster evolution depends on assumptions, such as: initial virial radius (r_v), and the IMF, that can affect either t_r or $\frac{\langle m \rangle}{m_i}$. Fig. 9 shows the difference in the evolution of two clusters (W and Wrv1) with different initial r_v and the overall spread in the IMF (Table 1). The initial average stellar mass for models W and Wrv1 are $\langle m \rangle = 0.66 M_\odot$ and $0.62 M_\odot$, respectively. The initial half-mass relaxation times for the models are 5.2 Gyr and 1.9 Gyr. Due to these differences, Wrv1 processes through its BHs much faster than W. Furthermore, Wrv1 retains significantly fewer N_{BH} , and evolves to a much denser and more compact final cluster than W.

We have also tested how changes in the binary fraction and binary properties of high-mass stars affect the overall cluster evolution. We find that with a fixed overall f_b , variations simply in $f_{b,\text{high}}$ and the distributions of orbital and companion properties for the high-mass binaries do not significantly affect the overall evolution of the clusters and their global observable properties.

5. BLACK HOLE BINARIES

To be detectable, either by observation of electromagnetic signals generated via accretion from a non-BH companion in a BH–non-BH binary (BH–nBH), or by detection of GWs from a BH–BH merger, BHs must be in binary systems. Here we explore the effects of our various initial assumptions on the number and properties of BBHs. Table 3 lists all our models and the corresponding numbers of single and binary BHs, retained and ejected from each cluster over its lifetime.

In general, we find that the number of BBHs (of any kind) in each of our model clusters is much lower compared to the total number of BHs (Table 3). Moreover, the BBH numbers are *not* strongly dependent on N_{BH} (Fig. 10). For example, depending on the assumptions in our models, we find a large range in the values of N_{BH} , varying from 0 to 935 at $t = 12$ Gyr. In contrast, at $t = 12$ Gyr the variation in the numbers of BH–BH ($N_{\text{BH–BH}}$) and BH–nBH ($N_{\text{BH–nBH}}$) binaries are 0 to 7 and 0 to 17, respectively. The correlation coefficient between N_{BH} and $N_{\text{BH–BH}}$ at $t = 12$ Gyr for all model clusters that did not get disrupted earlier than 12 Gyr is 0.56 and that between N_{BH} and $N_{\text{BH–nBH}}$ is 0.07. The low fraction of BBHs is true also for the BHs that are ejected from the clusters (Table 3).

These general trends are understandable from the basic process of how BBHs are created and dynamically processed inside dense star clusters. Almost all primordial binaries containing massive stars are disrupted inside a cluster. This is mainly due to orbital expansion via mass loss, which makes these binaries susceptible to disruption

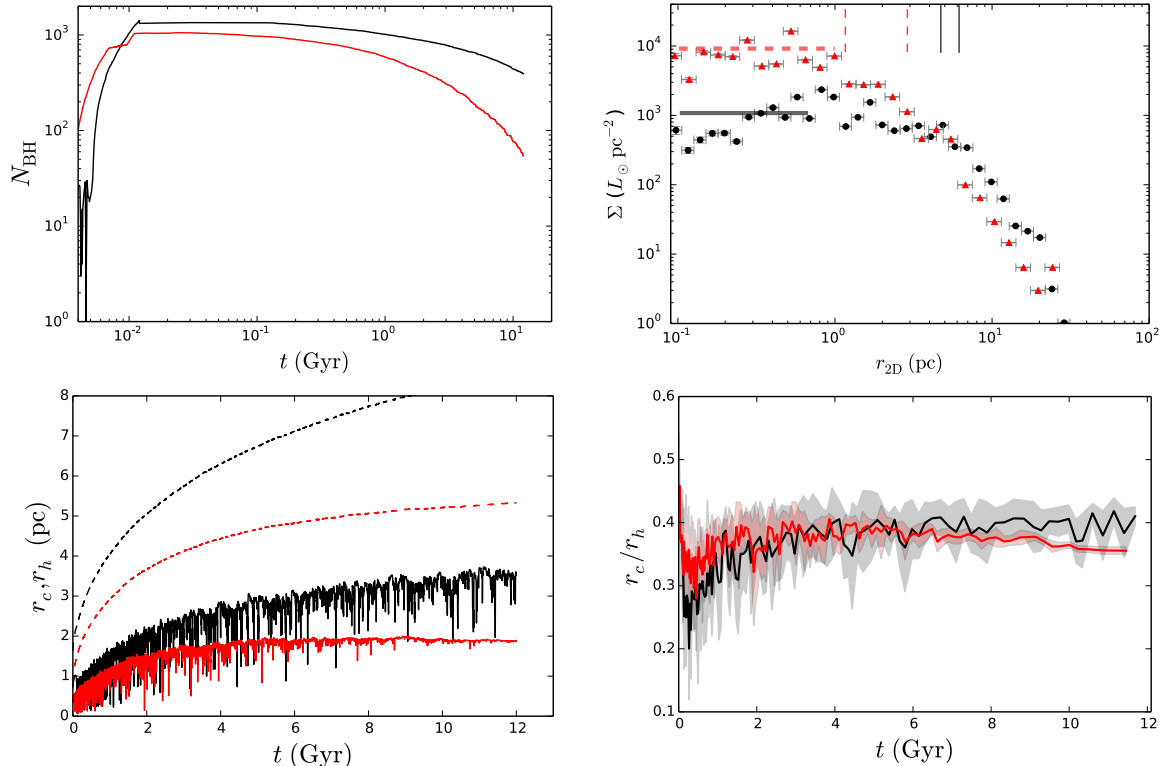


FIG. 9.— Same as Fig. 6, but comparing between models W (black) and Wrv1 (red; Table 1). The lower relaxation timescale and average stellar mass for model Wrv1 compared to model W leads to faster mass segregation, and as a result faster dynamical processing of BHs. The retained number of BHs N_{BH} in model cluster Wrv1 is significantly lower compared to N_{BH} in model cluster W. As a result, model cluster Wrv1 ceases to expand by $t = 12$ Gyr, and begins the relaxation-driven slow-contraction phase. In contrast, model cluster W keeps expanding till the end. Wrv1 appears as a higher-density and more compact cluster compared to W.

via subsequent strong scattering encounters (Fig. 11). Thus, most BHs in dense star clusters are singles. Almost all BBHs in dense star clusters, as well as BBHs that are ejected from them after $t \sim 10^2$ Myr, are binaries that are dynamically created in the dense cores of these clusters, and are *not* primordial. Note that even if an old star cluster typical of the present-day GCs now appears to have a low central density, its BHs likely have been processed in dramatically higher density environments as a result of repeated past BH-induced core collapse episodes (e.g., Figs. 1, 3, & 6). Both the values of $N_{\text{BH-BH}}$ and $N_{\text{BH-nBH}}$ in a cluster show large fluctuations over time and can vary between zero to ~ 10 (e.g., Figs. 11–14). This is reflective of the high frequency of dynamical processes that create and modify the BBHs in a dense star cluster, especially during a BH-driven core collapse. In these dense environments BBHs continuously form via three-body encounters, change via swapping of partners in binary-mediated scattering, get disrupted via strong scattering, and get ejected due to recoil from strong scattering encounters (e.g., Heggie 1975). The dynamical processes including disruption of primordial binaries, creation of new ones, and dynamical ejections essentially erase the binary properties the high-mass stars were born with. This in fact is the main difference between BBHs formed in a dense star cluster and BBHs that are born in isolation in the field. In the latter case, all BBHs are formed from primordial binaries, hence, the BBH properties as well as numbers relative to single stars are directly related to the assumptions of initial binary properties for

the high-mass stars.

While large numbers of BHs are still present in a star cluster, the core of the cluster is dominated by the BHs due to mass segregation. Internal dynamics determines how many of these BHs can hold onto their companions once formed via dynamics. As N_{BH} decreases, the BH-driven core collapses become less pronounced. As a result, a higher fraction of BHs can remain in binaries, and the ejection rate of BBHs decreases. Hence, although N_{BH} decreases, the fraction of BHs in BH–BH binaries increases, thus keeping $N_{\text{BH-BH}}$ largely unchanged (Fig 10). On the other hand, while N_{BH} is large, the very central regions are dominated by the (mostly) single BHs and lower-mass stars are driven out. A large N_{BH} also keeps the cluster puffed up, lowering the rate of encounters between BHs and binaries with non-BH members. Only after a cluster is sufficiently depleted of the BHs, can the rate of formation of BH–nBH binaries via exchange interactions involving a BH and a binary with non-BH members increase. However, at this stage the maximum $N_{\text{BH-nBH}}$ is likely limited by the low number of remaining BHs.

The lack of a strong correlation between N_{BH} and $N_{\text{BH-nBH}}$ has some interesting implications. For example, major efforts are now underway to detect BH candidates in GCs (e.g., Strader et al. 2012; Chomiuk et al. 2013; Strader et al. 2013; Miller-Jones et al. 2014b,a). For detection via electromagnetic signals (by comparing the radio and X-ray luminosities) there must be a BH with a non-BH accreting companion. For simplicity, if we

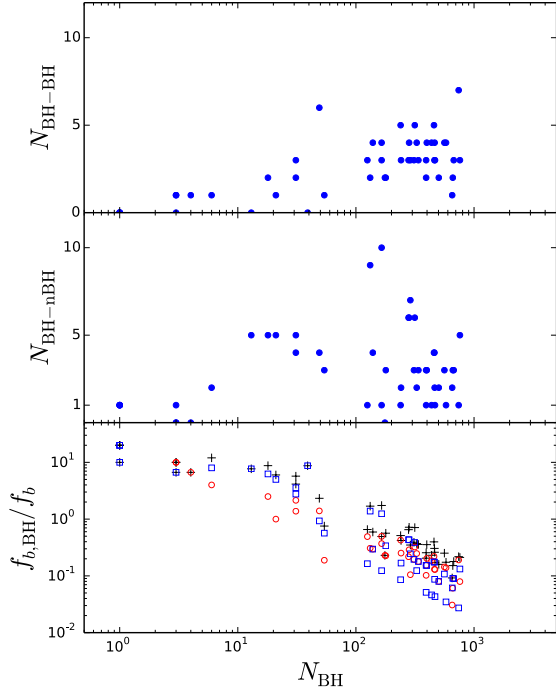


FIG. 10.— *Top*: The number of bound BHs N_{BH} vs the number of bound BH-BH binaries $N_{\text{BH-BH}}$. *Middle*: N_{BH} vs the number of bound BH-nBH binaries $N_{\text{BH-nBH}}$. *Bottom*: Binary fraction in BHs ($f_{b,\text{BH}}$) normalized by the overall binary fraction f_b . Pluses (black), circles (red), and squares (blue) denote the normalized binary fraction for all BH binaries, BH-BH binaries, and BH-nBH binaries, respectively. A larger fraction of BHs are in binaries relative to the overall binary fraction for models with low N_{BH} . High N_{BH} leads to BH-driven core-collapse which typically disrupts and ejects BH binaries. As N_{BH} decreases, BH-driven core-collapses stop occurring, reducing the efficiency of BBH destruction and ejection. BHs being the most massive objects, typically get exchanged into binaries via binary-mediated scattering encounters. As a result, the fraction of BHs in binaries increases as N_{BH} decreases.

treat $N_{\text{BH-nBH}}$ as a proxy for the absolute upper limit on the number of BH candidates that may be detectable via electromagnetic signatures, the lack of correlation between N_{BH} and $N_{\text{BH-nBH}}$ poses a serious challenge in inferring the number of total BHs in the GC from the discovery of BH candidates in that GC.

We now focus our attention on understanding the detailed evolution of BBHs inside a cluster and the effects of various initial assumptions through selected example models (Figs 11–14). Since we have shown that the assumed BH natal-kick distribution can bring dramatic changes to the overall cluster evolution, we first investigate the effects of BH formation kicks on the evolution of BBHs that are retained in the cluster (Fig. 11). The number of BBHs in the cluster is quite insensitive to the details of the kick distribution except for the case with $\sigma_{\text{BH}} = \sigma_{\text{NS}}$ (e.g., model K1). In the high-kick case, the large formation kicks essentially ejects most of the BHs from the cluster. The natal kicks are also large enough to disrupt all binaries during BH formation. Hence, not surprisingly, in the high-kick models, the values for $N_{\text{BH-BH}}$ as well as $N_{\text{BH-nBH}}$ are always low. Interestingly though, the number of BBHs is low even in our lowest kick models. For example, S which assumes a fallback-dependent momentum-conserving kick prescription and K3 which assumes that $\sigma_{\text{BH}} = 2.65 \text{ km s}^{-1}$, typically much lower

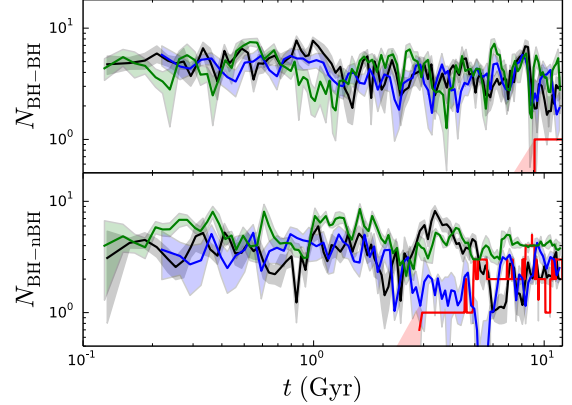


FIG. 11.— Evolution of the number of binary BHs bound to the cluster for different assumed natal kick distributions for BHs. Top and bottom panels show BH-BH and BH-nBH binary numbers. Both $N_{\text{BH-BH}}$ and $N_{\text{BH-nBH}}$ show large scatters over time. This is a direct consequence of the continuous disruption and ejection of existing binaries and dynamical formation of new ones at any given time in clusters. To reduce scatter we have under-sampled and show the mean (lines) and \pm one standard deviation (shaded region). Black, red, blue, and green denote models S, K1, K2, and K3, respectively (Table 1). Both $N_{\text{BH-BH}}$ and $N_{\text{BH-nBH}}$ remain low independent of the assumed distribution of natal kicks for BHs. This indicates that the softening of orbits for massive binaries due to mass loss via winds and compact object formation is responsible for dynamical disruption of most primordial binary orbits, and that this process does not depend on the natal kick distribution. Even with very low adopted natal kicks for BHs, $\sigma_{\text{BH}} = 2.65 \text{ km s}^{-1}$, K3 contains low numbers of binary BHs.

compared to orbital speeds of the massive binaries, both show low numbers of BBHs. As discussed earlier, the combined mass loss from stellar winds and compact object formation for high-mass stars expands the binary orbits and make them dynamically soft. Thus the majority of the high-mass binaries are disrupted independent of the magnitude of the SN kicks.

To further investigate this we compare two of our models that are identical in all aspects except the fraction of high-mass stars that are initially in binaries. To illustrate the limiting cases, Fig. 12 shows the evolution of retained BBHs for models F0 with initial $f_{b,\text{high}} = 0$ and F1 with initial $f_{b,\text{high}} = 1$ (§2.2; Table 1). Although initially the values of $N_{\text{BH-BH}}$ are vastly different between the models, within about 3 Gyr, they converge to essentially the same steady value in both models. However, $N_{\text{BH-nBH}}$ for the model with initial $f_{b,\text{high}} = 1$ is slightly lower compared to that in the model with initial $f_{b,\text{high}} = 0$ for $t > 5$ Gyr. This is likely due to the fact that to keep the overall f_b fixed at 0.05, the $f_{b,\text{high}} = 1$ case started with fewer low-mass stars in binaries compared to the $f_{b,\text{high}} = 0$ case. At late times, all BH-nBH binaries are dynamically formed via exchange interactions where a BH inserts itself into a binary by ejecting a non-BH component. Because of this, the relatively small number of low-mass stellar binaries in the $f_{b,\text{high}} = 1$ case (compared to $f_{b,\text{high}} = 0$ case) reduces the efficiency of new BH-nBH binary formation.

Similar trends are found by comparing models with differing prescriptions for stellar winds (Fig. 13). While the values of $N_{\text{BH-BH}}$ are very similar between clusters S and W, the lower final ρ_c in W results in production of a lower number of BH-nBH binaries compared to S at late times. This is consistent with our understanding

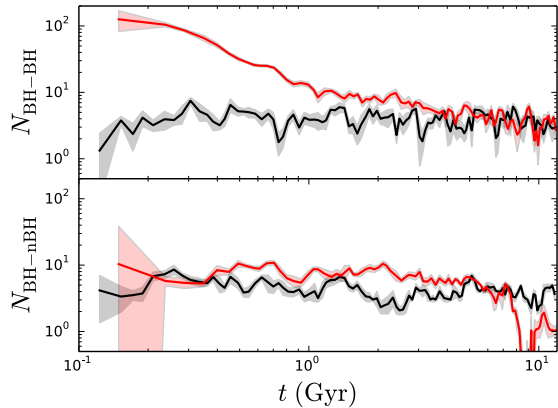


FIG. 12.— Same as Fig. 11 but showing a comparison between the evolution for two identical initial models differing only by the initial binary fraction in high-mass ($> 15 M_{\odot}$) stars, $f_{b,\text{high}}$. Black and red denote models F0 with initial $f_{b,\text{high}} = 0$ and F1 with initial $f_{b,\text{high}} = 1$, respectively (Table 1). In both cases, the overall binary fraction f_b is kept fixed at 0.05. Independent of the initial $f_{b,\text{high}}$, the final retained $N_{\text{BH-BH}}$ converge to a low value. The final retained $N_{\text{BH-nBH}}$ depends on the efficiency with which interactions involving BHs and binaries with non-BH components can produce BH-nBH binaries via exchange. The cluster with $f_{b,\text{high}} = 1$ has fewer low-mass binaries than the cluster with $f_{b,\text{high}} = 0$. As a result, BH-nBH binary formation is less effective in F1 compared to that in F0 at late times.

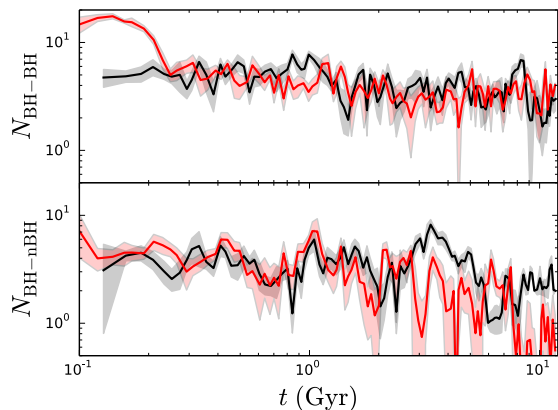


FIG. 13.— Same as Fig. 11 but compares between the evolution for two identical initial models differing by the assumed prescription for mass loss via stellar winds. Black and red denote models S with the strong and W with the weak wind prescriptions, respectively. The values of $N_{\text{BH-BH}}$ shows no difference between the two models. The value for $N_{\text{BH-nBH}}$ for the weak wind case is slightly lower compared to that for the strong wind case. Weak winds lead to more massive BHs, which in turn lead to more expanded clusters with lower central densities (e.g., Table 2). As a result, in the weak wind case, at late times formation of BH-nBH binaries via binary-mediated exchange interactions between single BHs and non-BH binaries is less efficient.

that most BH-nBH binaries retained in old clusters typical of the GCs are dynamically created. The dynamical age, mass-segregation timescale, and binary fraction can also moderately affect $N_{\text{BH-nBH}}$. The first two control N_{BH} in the cluster, and as a result the cluster’s dynamical properties and overall evolution. The initial binary fraction controls the number of binaries with no BH components that can take part in exchange interactions with single BHs and BH-BH binaries in old clusters. Fig. 14 compares $N_{\text{BH-BH}}$ and $N_{\text{BH-nBH}}$ for two models W

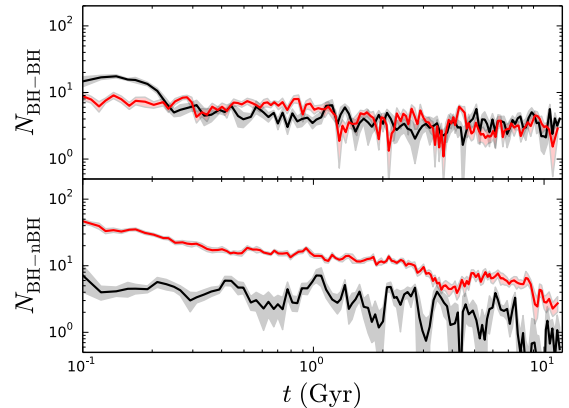


FIG. 14.— Same as Fig. 11 but showing a comparison between the evolution for two models differing by the overall binary fraction, r_v , and the IMF spread. Black and red denote models W and Wrv1, respectively (Table 1). The retained $N_{\text{BH-BH}}$ for both models converge within $t \approx 200$ Myr. The model cluster W with a lower initial f_b retains a lower $N_{\text{BH-nBH}}$ compared to Wrv1. (Tables 1, 3).

and Wrv1 that differ in their initial r_v , and f_b (Table 1). While $N_{\text{BH-BH}}$ converges to similar values within 200 Myr, Wrv1 with a higher f_b retains a larger number of BH-nBH binaries compared to W. In all cases, the fraction of BHs that are in binaries increases only after N_{BH} is sufficiently reduced (e.g., Fig. 10; also Table 3).

Independent of how many high-mass stars were born in binaries, cluster dynamics regulates the total number of BBHs retained in old GC-like clusters. Other variations in the binary orbital properties and $f_{b,\text{high}}$ (e.g., Sana et al. 2012) show the same general result. All knowledge of the primordial binary fraction and binary orbital properties of BHs or their progenitors is lost due to dynamical encounters in a star cluster. If massive stars were initially mostly in binary systems, these binaries would take part in strong dynamical encounters with other stars. These frequent scattering encounters either disrupt the binaries or eject them from the cluster. On the other hand, if initially BHs or their progenitors are not in binaries, new binaries can form dynamically. Through both channels the final number of BBHs attains small but similar values in all GCs (e.g., Table 3).

6. BINARY BLACK HOLE MERGERS

The BH-BH merger rates and properties of the BHs during merger in the local universe have been studied by multiple teams, either exploring the contributions from star clusters (e.g., Ziosi et al. 2014; Rodriguez et al. 2015, 2016a; Antonini et al. 2016) or from isolated binary stellar evolution in the field (e.g., Belczynski et al. 2014; Dominik et al. 2012, 2013; Belczynski et al. 2014; Dominik et al. 2015; Kowalska-Leszczynska et al. 2015; Belczynski et al. 2015). Here we focus on understanding the uncertainties associated with the BH-BH merger rates formed in clusters similar to the present-day GCs (e.g., Rodriguez et al. 2016a). As in earlier sections, we investigate how variations in initial assumptions affect the number of BH-BH mergers, merger times, and the properties of the binaries. The numbers of BH-BH mergers and the total masses of these mergers within two values of redshift (z) are listed in Table 3. Here we assume that each cluster is 12 Gyr old at the present day, and the red-

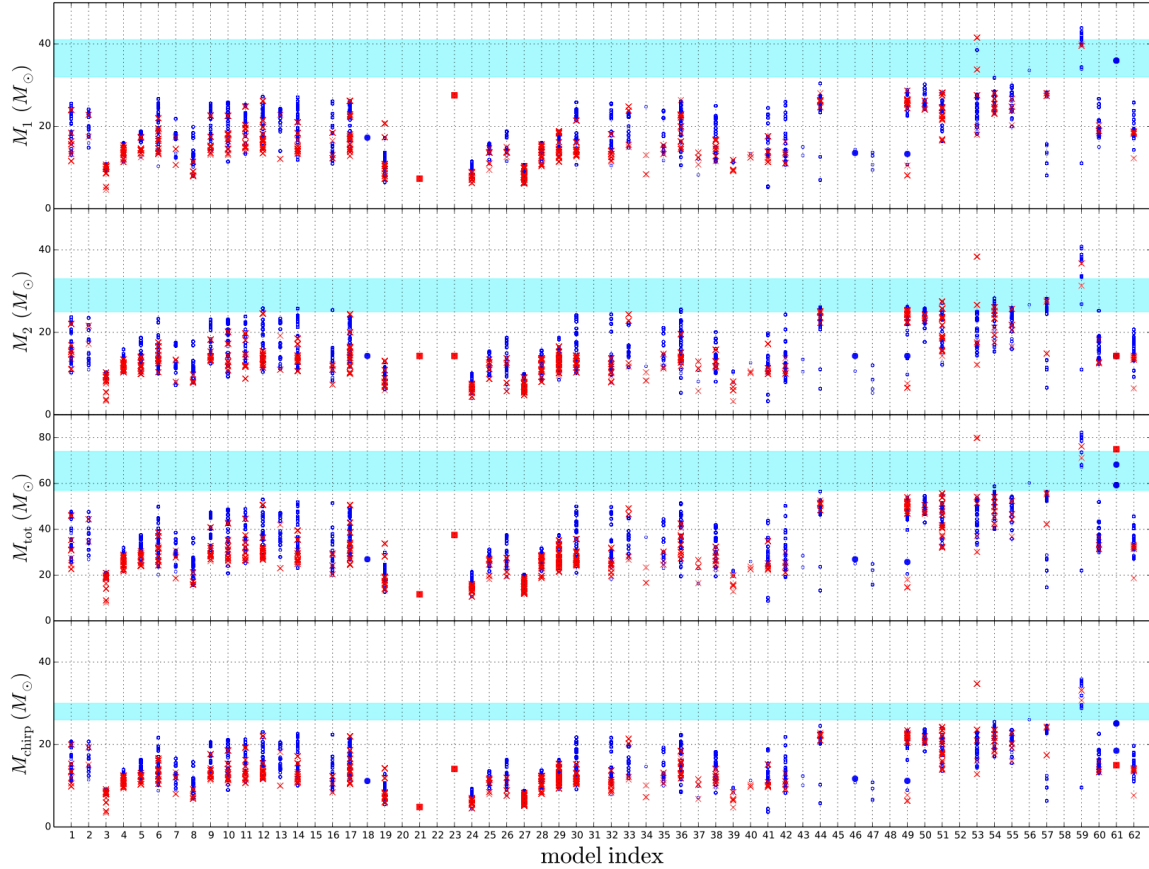


FIG. 15.— Top to bottom, the component masses ($M_{1,2}$), total mass (M_{tot}), and chirp mass (M_{chirp}) for BH-BH mergers within $0 \geq z \geq 0.2$ (blue) and $0.2 \geq z \geq 1$ (red) for each model identified by the serial number on the horizontal axis. Dots and crosses denote mergers after being ejected from the clusters. Circles and squares denote mergers within the clusters. Cyan shaded regions show GW150914 properties for reference. Weak winds help creating relatively more massive mergers. Assumptions of BH’s natal kicks and IMF affect number of mergers by changing the number of BHs that clusters can retain for dynamical processing, and the number of BHs produced for a given N , respectively.

shift corresponds to the lookback time of each merger.¹ To highlight the assumption relating t and z , we will refer to our model clusters as GCs in this context.

Fig. 15 shows the BH masses for all BH–BH mergers within $z = 0.2$ and 1 from all of our models, identified by the index numbers listed in Tables 1–3. Rodriguez et al. (2015, 2016a) found that the BH–BH mergers in the local universe ($z < 1$) is dominated by mergers that occur *after* the BH–BH binaries are ejected from their host GCs. This same result is generally found in our models independent of the details of the initial assumptions (Table 3). Now we highlight the assumptions that affect the number and properties of BH–BH mergers originating from GCs and occurring within some small z .

The largest effect arises from the assumed distribution of natal kicks for the BHs. We have already seen that independent of initial assumptions, primordial binaries involving BH-progenitor stars are generally disrupted (§5). All GCs modeled with an adopted BH natal kick distribution given by $\sigma_{\text{BH}} = \sigma_{\text{NS}}$ and no scaling based on fallback, eject almost all of their BHs due to the high natal kicks before they can dynamically form binaries. The handful of BH–BH binaries these GCs produce are all dynamically formed via binary-mediated strong scatter-

ing encounters within clusters at later times. As a result, when these GCs do produce BH–BH binaries that would merge in the local universe the mergers usually happen while the BH–BH binary is still bound to the GC.

The only other assumption explored in this study that can significantly impact the production of merging BH–BH binaries from GCs is the IMF. Any variations in the IMF for high-mass stars alters the number of mergers at $z < 1$ in a predictable manner. IMFs that produce more high-mass stars produce more BHs, and the number of BH–BH mergers in the local universe increases accordingly. For example, the IMF with $\alpha_1 = 1.6$, for a given initial N forms much higher numbers of BHs compared to models with larger α_1 . Even models with the largest natal kicks for the BHs may produce significant numbers of BH–BH mergers if $\alpha_1 = 1.6$ is assumed. Of course, for the same reason, a combination of flat high-end for the IMF and low natal kicks for BHs can significantly increase the number of mergers within $z < 1$. Nevertheless, note that we find that all clusters modeled with $\alpha_1 = 1.6$ get disrupted long before they are 12 Gyr old, a typical age for the MW GCs, due to a combination of mass loss and energy production via BH dynamics from the large numbers of high-mass stars that such an IMF produces. As a result, this extreme low value of α_1 seems very unlikely in reality. Similarly, if the IMF mass range

¹ We assume $h = 0.677$, $\Omega_M = 0.309$, $\Omega_K = 0.$, and $\Omega_L = 0.691$.

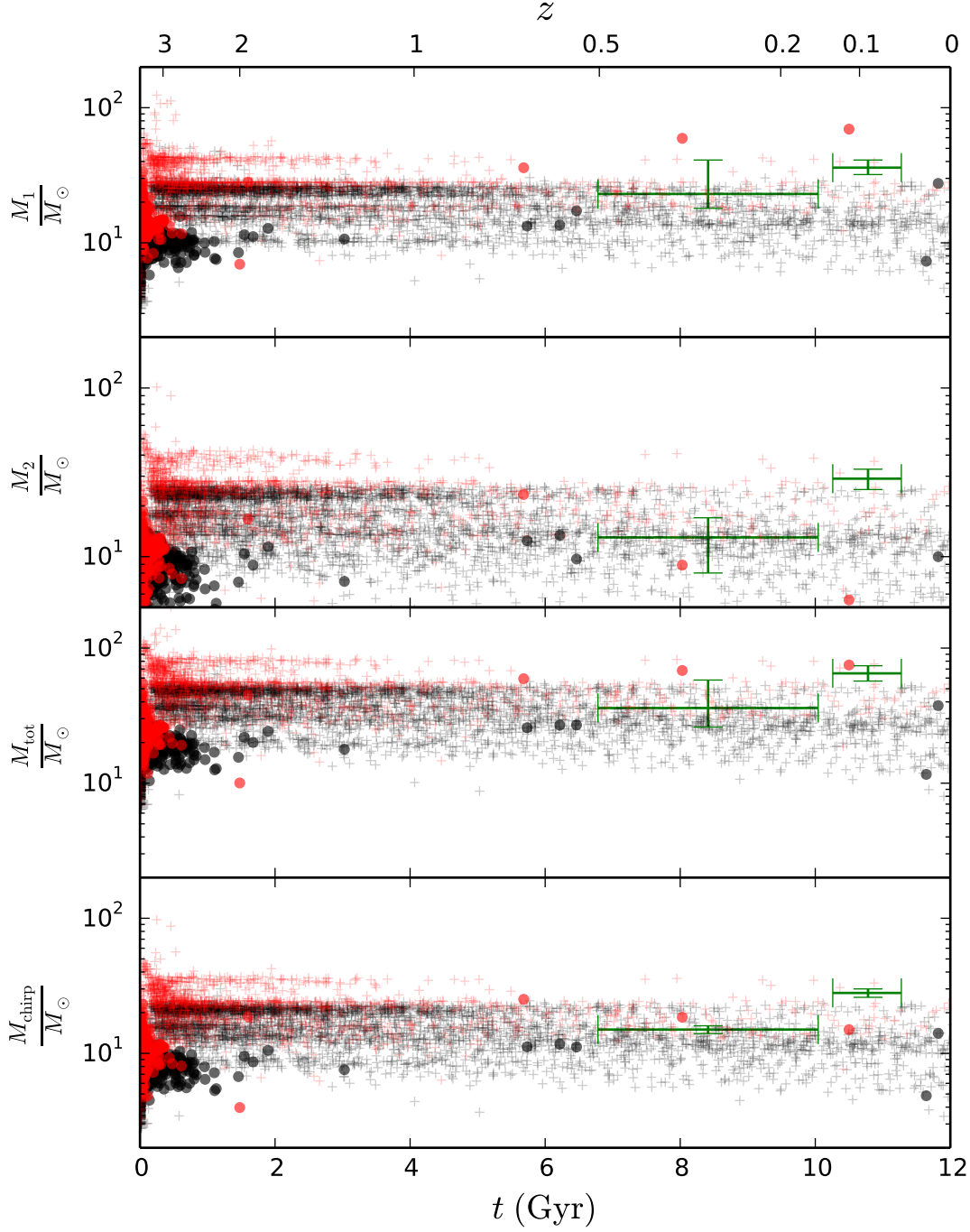


FIG. 16.— Top to bottom, the component masses ($M_{1,2}$), total mass (M_{tot}), and chirp mass (M_{chirp}) for BH-BH mergers as a function of merger time. The top axis shows the lookback redshift z assuming that $t = 12$ Gyr is equivalent to $z = 0$. Pluses, and circles denote mergers that happen after the BH-BH binaries are ejected from the host clusters, and BH-BH mergers that happen while the binaries are still bound to the host clusters. The reported gravitational wave observation GW150914 and the trigger event LVT151012 are shown with errorbars in green for reference. Black and red denote BH-BH mergers from models assuming the strong and weak wind prescriptions, respectively. Most BH-BH mergers in the local universe happen after the binaries are ejected from the host clusters. BH-BH binaries that merge inside clusters typically have lower masses compared to those that merge after being ejected. Weak winds are necessary for producing BH-BH mergers as massive as GW150914 for the metallicities we consider. Most mergers in our models are closer to the properties of LVT151012.

is extended to lower-mass stars, the number of BHs produced, and as a result, the number of BH–BH mergers is reduced.

While the distribution of natal kicks and the assumed IMF may change the actual number of BH–BH mergers from GCs within a given z , the masses of the binary mergers depend on neither. Instead, the mass distribution of the merging BHs is primarily determined by the assumed stellar winds for a given metallicity Z , which we controlled by using either the weak or strong wind prescriptions in this study (§2.5). Fig. 16 shows the component masses ($M_{1,2}$), total mass (M_{tot}) and chirp mass (M_{chirp}) of all BH–BH mergers within 12 Gyr from all our models as a function of their merger times. We divide all model GCs in two groups based on the two wind prescriptions we consider. GCs modeled with weak winds produce more massive merging BH–BH binaries compared to those modeled with strong winds. In particular, GCs modeled assuming weak stellar winds are the only ones that can produce BH–BH mergers with masses similar to GW150914 for the metallicities we consider. Nevertheless, we find that the majority of BH–BH binaries merging within $z = 0.2$ even from model GCs assuming weak winds have lower BH masses than the component masses of GW150914 (Table 1). The BH masses of the other reported trigger event LVT151012 are more common in the BH–BH mergers found in our models. GCs modeled with both strong and weak winds can produce BH–BH mergers similar in properties to LVT151012. Very few of the BH–BH mergers in the local universe are expected to happen while the binary is still bound to the host GC. Most BH–BH binaries that merge while bound to the GC do so at early times, and typically have lower masses than those that merge after ejection. Since, the higher the mass of the BHs, the earlier it is ejected from the cluster (e.g., Morscher et al. 2015), the mergers after ejection are typically more massive compared to those that happen within a cluster.

Note that throughout this section we have assumed that $z = 0$ is equivalent to $t = 12$ Gyr keeping, in particular, the MW GCs in mind. Of course depending on the relation between t and z , which in terms of astrophysics is determined by the current age of the clusters that produce the BHs, the number of BH–BH mergers, their masses, and the relative importance of mergers within a cluster and mergers after being ejected from the cluster can change (Fig. 16).

7. SUMMARY AND DISCUSSION

In this study we have explored how identical initial clusters can diverge in their evolution depending on various ill-constrained initial assumptions affecting the high-mass stars, including the high-end slope (α_1) of the IMF, the distribution of natal kicks for BHs, the binary fraction and the binary orbital properties for massive stars, and the prescriptions adopted for stellar winds. Using Monte Carlo simulations we have studied the effects of each of these assumptions from three different perspectives: (1) how they affect the global evolution of star clusters and their final observable properties; (2) how they affect the binary fraction of BHs and the numbers of different types of BH binaries; and (3) how these assumptions affect the number and properties of merging BH–BH binaries that could be detected as GW sources.

We find that, even when we start from the same initial cluster model, variations in these initial assumptions can alter the number of retained BHs, N_{BH} , at any given time by orders of magnitude (e.g., Tables 2, 3). This difference in N_{BH} can then change the overall dynamical evolution of the host star cluster, dramatically altering its lifetime and, if it survives to the present, its final observable properties (Figs 4–9).

In contrast, the total number and properties of BH–BH and BH–nBH binaries retained inside old star clusters are not significantly affected by varying any of these assumptions. Through dynamical interactions in the dense cluster cores or kicks at compact object formation, all primordial binaries containing BH progenitors are quickly disrupted. On the relaxation timescale, binaries are reformed dynamically and eventually both the number and properties of retained binaries with at least one BH component are determined entirely by stellar dynamical processes. As N_{BH} decreases, the fraction of BHs in binaries increases, so that $N_{\text{BH–nBH}}$ and $N_{\text{BH–BH}}$ in old clusters do not strongly correlate with N_{BH} . This has important implications for inferring N_{BH} in clusters where BH XRB candidates have been identified. In general we find that observable cluster properties including $r_{c,\text{obs}}$ and $\Sigma_{c,\text{obs}}$ are better indicators of N_{BH} compared to $N_{\text{BH–nBH}}$ (Figs. 4, 5, & 10).

The number of BH–BH mergers from clusters in the local universe is only affected by the assumptions made about BH natal kicks and the stellar IMF (Fig. 15, Table 3). This is very different from the situation encountered in binary population synthesis studies for field binaries, where a myriad of assumptions (e.g., about the initial properties of binaries) and uncertain stellar evolution parameters (e.g., the infamous common-envelope efficiency α_{CE}) can change results by orders of magnitude. Instead, far more robust theoretical predictions can be made for merging BH–BH binaries that are dynamically produced in dense star clusters.

If BHs receive natal kicks as large as neutron stars formed in core-collapsed SN, the expected number of BH–BH mergers becomes very small, simply because almost all BHs are ejected from the cluster at birth. Note, however, that with such large kicks the number of BH–BH binaries generated in star clusters is significantly higher than in the field, where BHs can never again acquire a binary companion if natal kicks disrupt the primordial binaries they were born in (see Rodriguez et al. 2016a, for comparative rate estimates between star clusters and the field assuming high and low natal kicks for BHs). Variations in the assumed IMF slope change the number of BH–BH mergers in clusters in a predictable way, simply by changing the relative proportion of high-mass stars (see §6, Fig. 15). The component masses and total masses (or equivalently the chirp masses) of merging BH–BH binaries are affected only by the assumed prescription for stellar-wind mass loss. Other parameters such as $f_{b,\text{high}}$ or any of the initial properties of massive binaries (e.g., the distributions of mass ratios and orbital periods) have no effect at all (Fig. 15, Table 3).

In the context of GW detection, we therefore expect the BH–BH merger rates and properties estimated in Rodriguez et al. (2015, 2016a) for dynamically produced binaries to be quite robust, and in particular to remain unaffected by any change in assumptions concerning the

initial distributions of binary properties or the binary stellar evolution. In contrast, the BH–BH merger rates estimated for isolated field binaries (e.g., Belczynski et al. 2015; Dominik et al. 2013, 2015) depend directly and sensitively on many assumptions concerning the details of stellar evolution (mass transfer, tidal dissipation effects, common envelopes) and on the assumed distributions of initial properties for high-mass binaries. In addition, the assumption of truly isolated binary evolution may be suspect because most stars and binaries currently in the field were still originally formed in clusters, which later dissolved (e.g., Carpenter 2000; Lada & Lada 2003; Porras et al. 2003; Portegies Zwart et al. 2010), and binaries

may have been affected by dynamical interactions before their release into the field (e.g., Ziosi et al. 2014).

We are grateful to Vicky Kalogera for her helpful comments. This work was supported by NASA ATP Grant NNX14AP92G and NSF Grant AST1312945. S.C. also acknowledges support from the National Aeronautics and Space Administration through Chandra Award Number TM5-16004X/NAS8-03060 issued by the Chandra X-ray Observatory Center, which is operated by the Smithsonian Astrophysical Observatory for and on behalf of the National Aeronautics Space Administration under contract NAS8-03060.

REFERENCES

- Aarseth, S. J. 2010, *Gravitational N-Body Simulations* — 2012, *MNRAS*, 422, 841
- Abbott, B. P., Abbott, R., Abbott, T. D., Abernathy, M. R., Acernese, F., & LIGO Scientific Collaboration and Virgo Collaboration. 2016a, *Phys. Rev. Lett.*, 116, 061102
- Abbott, B. P., Abbott, R., Abbott, T. D., Abernathy, M. R., Acernese, F., Ackley, K., Adams, C., Adams, T., Addesso, P., Adhikari, R. X., B., V., & LIGO Scientific Collaboration and Virgo Collaboration. 2016b, *ApJ*, 818, L22
- Altamirano, D., Patruno, A., Heinke, C. O., Markwardt, C., Strohmayer, T. E., Linares, M., Wijnands, R., van der Klis, M., & Swank, J. H. 2010, *ApJ*, 712, L58
- Altamirano, D., Wijnands, R., Heinke, C. O., Sivakoff, G. R., & Pooley, D. 2012, *The Astronomer’s Telegram*, 4264, 1
- Antonini, F., Chatterjee, S., Rodriguez, C. L., Morscher, M., Pattabiraman, B., Kalogera, V., & Rasio, F. A. 2016, *ApJ*, 816, 65
- Belczynski, K., Bulik, T., Fryer, C. L., Ruiter, A., Valsecchi, F., Vink, J. S., & Hurlley, J. R. 2010a, *ApJ*, 714, 1217
- Belczynski, K., Buonanno, A., Cantiello, M., Fryer, C. L., Holz, D. E., Mandel, I., Miller, M. C., & Walczak, M. 2014, *ApJ*, 789, 120
- Belczynski, K., Dominik, M., Bulik, T., O’Shaughnessy, R., Fryer, C., & Holz, D. E. 2010b, *ApJ*, 715, L138
- Belczynski, K., Kalogera, V., & Bulik, T. 2002, *ApJ*, 572, 407
- Belczynski, K., Repetto, S., Holz, D., O’Shaughnessy, R., Bulik, T., Berti, E., Fryer, C., & Dominik, M. 2015, *ArXiv e-prints*
- Bozzo, E., Ferrigno, C., Stevens, J., Belloni, T. M., Rodriguez, J., den Hartog, P. R., Papitto, A., Kreykenbohm, I., Fontani, F., & Gibaud, L. 2011, *A&A*, 535, L1
- Brandt, W. N., Podsiadlowski, P., & Sigurdsson, S. 1995, *MNRAS*, 277, L35
- Breen, P. G. & Hoggie, D. C. 2013, *MNRAS*, 432, 2779
- Carpenter, J. M. 2000, *AJ*, 120, 3139
- Chatterjee, S., Fregeau, J. M., Umbreit, S., & Rasio, F. A. 2010, *ApJ*, 719, 915
- Chatterjee, S., Rasio, F. A., Sills, A., & Glebbeek, E. 2013a, *ApJ*, 777, 106
- Chatterjee, S., Umbreit, S., Fregeau, J. M., & Rasio, F. A. 2013b, *MNRAS*, 429, 2881
- Chernoff, D. F. & Weinberg, M. D. 1990, *ApJ*, 351, 121
- Chomiuk, L., Strader, J., Maccarone, T. J., Miller-Jones, J. C. A., Heinke, C., Noyola, E., Seth, A. C., & Ransom, S. 2013, *ApJ*, 777, 69
- Cordes, J. M., Romani, R. W., & Lundgren, S. C. 1993, *Nature*, 362, 133
- de Boer, K. S., Tucholke, H.-J., & Schmidt, J. H. K. 1997, *A&A*, 317, L23
- Dhawan, V., Mirabel, I. F., Ribó, M., & Rodrigues, I. 2007, *ApJ*, 668, 430
- Dominik, M., Belczynski, K., Fryer, C., Holz, D. E., Berti, E., Bulik, T., Mandel, I., & O’Shaughnessy, R. 2012, *ApJ*, 759, 52
- 2013, *ApJ*, 779, 72
- Dominik, M., Berti, E., O’Shaughnessy, R., Mandel, I., Belczynski, K., Fryer, C., Holz, D. E., Bulik, T., & Panarale, F. 2015, *ApJ*, 806, 263
- Fragos, T., Willems, B., Kalogera, V., Ivanova, N., Rockefeller, G., Fryer, C. L., & Young, P. A. 2009, *ApJ*, 697, 1057
- Fregeau, J. M., Gürkan, M. A., Joshi, K. J., & Rasio, F. A. 2003, *ApJ*, 593, 772
- Fryer, C. L. & Kalogera, V. 2001, *ApJ*, 554, 548
- Gualandris, A., Colpi, M., Portegies Zwart, S., & Possenti, A. 2005, *ApJ*, 618, 845
- Gürkan, M. A., Freitag, M., & Rasio, F. A. 2004, *ApJ*, 604, 632
- Hénon, M. H. 1971, *Ap&SS*, 14, 151
- Hoggie, D. & Hut, P. 2003, *The Gravitational Million-Body Problem: A Multidisciplinary Approach to Star Cluster Dynamics*
- Hoggie, D. C. 1975, *MNRAS*, 173, 729
- Hurlley, J. R., Pols, O. R., & Tout, C. A. 2000, *MNRAS*, 315, 543
- Hurlley, J. R., Tout, C. A., & Pols, O. R. 2002, *MNRAS*, 329, 897
- Irwin, J. A., Brink, T. G., Bregman, J. N., & Roberts, T. P. 2010, *ApJ*, 712, L1
- Joshi, K. J., Nave, C. P., & Rasio, F. A. 2001, *ApJ*, 550, 691
- Joshi, K. J., Rasio, F. A., & Portegies Zwart, S. 2000, *ApJ*, 540, 969
- Kalogera, V., King, A. R., & Rasio, F. A. 2004, *ApJ*, 601, L171
- King, I. 1962, *AJ*, 67, 471
- King, I. R. 1965, *AJ*, 70, 376
- 1966, *AJ*, 71, 64
- Kowalska-Leszczynska, I., Regimbau, T., Bulik, T., Dominik, M., & Belczynski, K. 2015, *A&A*, 574, A58
- Kroupa, P. 2001, *MNRAS*, 322, 231
- Kroupa, P. & Boily, C. M. 2002, *MNRAS*, 336, 1188
- Kulkarni, S. R., Hut, P., & McMillan, S. 1993, *Nature*, 364, 421
- Kundu, A., Maccarone, T. J., & Zepf, S. E. 2002, *ApJ*, 574, L5
- Lada, C. J. & Lada, E. A. 2003, *ARA&A*, 41, 57
- Lewin, W. H. G. & van der Klis, M. 2006, *Compact Stellar X-ray Sources*
- Lyne, A. G. & Lorimer, D. R. 1994, *Nature*, 369, 127
- Maccarone, T. J., Kundu, A., Zepf, S. E., & Rhode, K. L. 2007, *Nature*, 445, 183
- Mackey, A. D., Wilkinson, M. I., Davies, M. B., & Gilmore, G. F. 2008, *MNRAS*, 386, 65
- Miller-Jones, J., Maccarone, T., Chomiuk, L., Strader, J., Bogdanov, S., Sivakoff, G., & Heinke, C. 2014a, *A new black hole candidate in the globular cluster 47 Tucanae*, *ATNF Proposal*
- Miller-Jones, J., Maccarone, T., Chomiuk, L., Strader, J., Sivakoff, G., Heinke, C., Shishkovsky, L., & Huizenga, D. 2014b, *A comprehensive ATCA survey for black holes in southern globular clusters*, *ATNF Proposal*
- Moody, K. & Sigurdsson, S. 2009, *ApJ*, 690, 1370
- Morscher, M., Pattabiraman, B., Rodriguez, C., Rasio, F. A., & Umbreit, S. 2015, *ApJ*, 800, 9
- Morscher, M., Umbreit, S., Farr, W. M., & Rasio, F. A. 2013, *ApJ*, 763, L15
- Nelemans, G., Tauris, T. M., & van den Heuvel, E. P. J. 1999, *A&A*, 352, L87
- Noyola, E. & Gebhardt, K. 2006, *AJ*, 132, 447
- Pattabiraman, B., Umbreit, S., Liao, W.-k., Choudhary, A., Kalogera, V., Memik, G., & Rasio, F. A. 2013, *ApJS*, 204, 15
- Pejcha, O. & Thompson, T. A. 2015, *ApJ*, 801, 90

TABLE 1
 INITIAL MODEL PARAMETERS.

No.	Name	M ($10^5 M_\odot$)	r_G (kpc)	f_b	Z	r_v (pc)	BH-formation kick		High-mass Binaries			IMF	
							$\frac{\sigma_{\text{BH}}}{\sigma_{\text{NS}}}$	FB	$f_{b,\text{high}}$	q range	$\frac{dn}{d \log P}$	range	α_1
1	S	5.2	8	0.05	0.001	2	1	y	0.05	[0.1/ m_p , 1]	P^0	[0.1, 100]	2.3
2	SR1Z	5.2	8	0.05	0.001	2	1	y	0.05	[0.1/ m_p , 1]	P^0	[0.1, 100]	2.3
3	SR1	5.2	1	0.05	0.02	2	1	y	0.05	[0.1/ m_p , 1]	P^0	[0.1, 100]	2.3
4	SR2	5.2	2	0.05	0.007	2	1	y	0.05	[0.1/ m_p , 1]	P^0	[0.1, 100]	2.3
5	SR4	5.2	4	0.05	0.003	2	1	y	0.05	[0.1/ m_p , 1]	P^0	[0.1, 100]	2.3
6	SR20	5.2	20	0.05	0.0003	2	1	y	0.05	[0.1/ m_p , 1]	P^0	[0.1, 100]	2.3
7	SIwfb0.1	4.9	8	0.1	0.001	2	1	y	0.05	[0.1/ m_p , 1]	P^0	[0.08, 150]	2.3
8	SIwfb0.1rv1	4.9	8	0.1	0.001	1	1	y	0.05	[0.1/ m_p , 1]	P^0	[0.08, 150]	2.3
9	FO	5.2	8	0.05	0.001	2	1	y	0	-	-	[0.1, 100]	2.3
10	F1	5.6	8	0.05	0.001	2	1	y	1	[0.1/ m_p , 1]	P^0	[0.1, 100]	2.3
11	FO.7Ms0.1	5.5	8	0.05	0.001	2	1	y	0.7	[0.1/ m_p , 1]	$P^{-0.55}$	[0.1, 100]	2.3
12	FO.7q0.6	5.6	8	0.05	0.001	2	1	y	0.7	[0.6, 1]	$P^{-0.55}$	[0.1, 100]	2.3
13	FO.7q0.6R1	5.6	1	0.05	0.001	2	1	y	0.7	[0.6, 1]	$P^{-0.55}$	[0.1, 100]	2.3
14	FO.7q0.6R3	5.6	3	0.05	0.001	2	1	y	0.7	[0.6, 1]	$P^{-0.55}$	[0.1, 100]	2.3
15	K1	5.2	8	0.05	0.001	2	1	n	0.05	[0.1/ m_p , 1]	P^0	[0.1, 100]	2.3
16	K2	5.2	8	0.05	0.001	2	0.1	n	0.05	[0.1/ m_p , 1]	P^0	[0.1, 100]	2.3
17	K3	5.2	8	0.05	0.001	2	0.01	n	0.05	[0.1/ m_p , 1]	P^0	[0.1, 100]	2.3
18	SIwfb0.1rv1K1	4.9	8	0.1	0.001	1	1	n	0.05	[0.1/ m_p , 1]	P^0	[0.08, 150]	2.3
19	SIwfb0.1rv1K3	4.9	8	0.1	0.001	1	0.01	n	0.05	[0.1/ m_p , 1]	P^0	[0.08, 150]	2.3
20	K1R1	5.2	1	0.05	0.02	2	1	n	0.05	[0.1/ m_p , 1]	P^0	[0.1, 100]	2.3
21	K1R2	5.2	2	0.05	0.007	2	1	n	0.05	[0.1/ m_p , 1]	P^0	[0.1, 100]	2.3
22	K1R4	5.2	4	0.05	0.003	2	1	n	0.05	[0.1/ m_p , 1]	P^0	[0.1, 100]	2.3
23	K1R20	5.2	20	0.05	0.0003	2	1	n	0.05	[0.1/ m_p , 1]	P^0	[0.1, 100]	2.3
24	K2R1	5.2	1	0.05	0.02	2	0.1	n	0.05	[0.1/ m_p , 1]	P^0	[0.1, 100]	2.3
25	K2R2	5.2	2	0.05	0.007	2	0.1	n	0.05	[0.1/ m_p , 1]	P^0	[0.1, 100]	2.3
26	K2R4	5.2	4	0.05	0.003	2	0.1	n	0.05	[0.1/ m_p , 1]	P^0	[0.1, 100]	2.3
27	K3R1	5.2	1	0.05	0.02	2	0.01	n	0.05	[0.1/ m_p , 1]	P^0	[0.1, 100]	2.3
28	K3R2	5.2	2	0.05	0.007	2	0.01	n	0.05	[0.1/ m_p , 1]	P^0	[0.1, 100]	2.3
29	K3R4	5.2	4	0.05	0.003	2	0.01	n	0.05	[0.1/ m_p , 1]	P^0	[0.1, 100]	2.3
30	K3R20	5.2	20	0.05	0.0003	2	0.01	n	0.05	[0.1/ m_p , 1]	P^0	[0.1, 100]	2.3
31	K1R1Z	5.2	1	0.05	0.001	2	1	n	0.05	[0.1/ m_p , 1]	P^0	[0.1, 100]	2.3
32	K2R1Z	5.2	1	0.05	0.001	2	0.1	n	0.05	[0.1/ m_p , 1]	P^0	[0.1, 100]	2.3
33	K3R1Z	5.2	1	0.05	0.001	2	0.01	n	0.05	[0.1/ m_p , 1]	P^0	[0.1, 100]	2.3
34	FO.7Ms0.1K1	5.5	8	0.05	0.001	2	1	n	0.7	[0.1/ m_p , 1]	$P^{-0.55}$	[0.1, 100]	2.3
35	FO.7Ms0.1K2	5.5	8	0.05	0.001	2	0.1	n	0.7	[0.1/ m_p , 1]	$P^{-0.55}$	[0.1, 100]	2.3
36	FO.7Ms0.1K3	5.5	8	0.05	0.001	2	0.01	n	0.7	[0.1/ m_p , 1]	$P^{-0.55}$	[0.1, 100]	2.3
37	FO.7q0.6K1	5.6	8	0.05	0.001	2	1	n	0.7	[0.6, 1]	$P^{-0.55}$	[0.1, 100]	2.3
38	FO.7q0.6K2	5.6	8	0.05	0.001	2	0.1	n	0.7	[0.6, 1]	$P^{-0.55}$	[0.1, 100]	2.3
39	FO.7q0.6K1R1	5.6	1	0.05	0.001	2	0.01	n	0.7	[0.6, 1]	$P^{-0.55}$	[0.1, 100]	2.3
40	FO.7q0.6K1R3	5.6	3	0.05	0.001	2	0.01	n	0.7	[0.6, 1]	$P^{-0.55}$	[0.1, 100]	2.3
41	FO.7q0.6K2R1	5.6	1	0.05	0.001	2	0.01	n	0.7	[0.6, 1]	$P^{-0.55}$	[0.1, 100]	2.3
42	FO.7q0.6K2R3	5.6	3	0.05	0.001	2	0.01	n	0.7	[0.6, 1]	$P^{-0.55}$	[0.1, 100]	2.3
43	Is	3.6	8	0.05	0.001	2	1	n	0.05	[0.1/ m_p , 1]	P^0	[0.1, 100]	3.0
44	If	16.1	8	0.05	0.001	2	1	n	0.05	[0.1/ m_p , 1]	P^0	[0.1, 100]	1.6
45	IsK1	3.6	8	0.05	0.001	2	1	n	0.05	[0.1/ m_p , 1]	P^0	[0.1, 100]	3.0
46	IsK2	3.6	8	0.05	0.001	2	0.1	n	0.05	[0.1/ m_p , 1]	P^0	[0.1, 100]	3.0
47	IsK3	3.6	8	0.05	0.001	2	0.01	n	0.05	[0.1/ m_p , 1]	P^0	[0.1, 100]	3.0
48	IfK1	16.1	8	0.05	0.001	2	1	n	0.05	[0.1/ m_p , 1]	P^0	[0.1, 100]	1.6
49	IfK2	16.1	8	0.05	0.001	2	0.1	n	0.05	[0.1/ m_p , 1]	P^0	[0.1, 100]	1.6
50	IfK3	16.1	8	0.05	0.001	2	0.01	n	0.05	[0.1/ m_p , 1]	P^0	[0.1, 100]	1.6
51	W	5.2	8	0.05	0.001	2	1	y	0.05	[0.1/ m_p , 1]	P^0	[0.1, 100]	2.3
52	WK1	5.2	8	0.05	0.001	2	1	n	0.05	[0.1/ m_p , 1]	P^0	[0.1, 100]	2.3
53	WK2	5.2	8	0.05	0.001	2	0.1	n	0.05	[0.1/ m_p , 1]	P^0	[0.1, 100]	2.3
54	WK3	5.2	8	0.05	0.001	2	0.01	n	0.05	[0.1/ m_p , 1]	P^0	[0.1, 100]	2.3
55	WFO.7q0.6	5.6	8	0.05	0.001	2	1	y	0.7	[0.6, 1]	$P^{-0.55}$	[0.1, 100]	2.3
56	WFO.7q0.6K1	5.6	8	0.05	0.001	2	1	n	0.7	[0.6, 1]	$P^{-0.55}$	[0.1, 100]	2.3
57	WIf	16.1	8	0.05	0.001	2	1	y	0.05	[0.1/ m_p , 1]	P^0	[0.1, 100]	1.6
58	WIfK1	16.1	8	0.05	0.001	2	1	n	0.05	[0.1/ m_p , 1]	P^0	[0.1, 100]	1.6
59	WIfK3	16.1	8	0.05	0.001	2	0.01	n	0.05	[0.1/ m_p , 1]	P^0	[0.1, 100]	1.6
60	Wrv1	5.0	8	0.1	0.001	1	1	y	0.1	[0.1/ m_p , 1]	P^0	[0.08, 150]	2.3
61	Wrv1K1	5.0	8	0.1	0.001	1	1	n	0.1	[0.1/ m_p , 1]	P^0	[0.08, 150]	2.3
62	Wrv1K3	5.0	8	0.1	0.001	1	0.01	n	0.1	[0.1/ m_p , 1]	P^0	[0.08, 150]	2.3

 NOTE. — Each model initially has $N = 8 \times 10^5$ stars. Column FB denotes whether or not natal kicks for BHs are dependent on fallback. α_1 denotes the magnitude of the power-law exponent for stars of initial mass $> 1 M_\odot$. q -distribution is always uniform.

TABLE 2
FINAL STRUCTURAL PROPERTIES OF MODEL CLUSTERS.

No.	t (Gyr)	N (10^4)	M ($10^4 M_\odot$)	f_b	$f_{b,c}$	r_c	$r_{c,obs}$	r_h	$r_{hl,obs}$	ρ_c ($10^3 M_\odot/\text{pc}^3$)	$\Sigma_{c,obs}$ ($10^3 L_\odot/\text{pc}^2$)	$v_{\sigma,c}$	$v_{\sigma,c,obs}$ (km s^{-1})
								(pc)					
1	12.0	71	26	0.05	0.05	2.90	3.06	7.89	5.55	17.8	1.9	9.8	3.40
2	≈ 5												
3	12.0	24	12	0.06	0.13	0.64	0.40	2.80	1.41	44.0	31.5	10.9	4.26
4	12.0	55	21	0.05	0.06	2.52	2.86	6.12	4.01	9.1	2.2	9.8	3.32
5	12.0	68	25	0.05	0.06	2.83	2.59	7.16	4.73	12.3	2.0	9.9	3.46
6	12.0	73	27	0.05	0.05	3.07	4.22	8.54	6.24	21.8	1.5	9.7	3.30
7	12.0	76	26	0.09	0.12	1.89	1.12	5.65	3.27	7.5	9.2	11.5	4.37
8	12.0	71	25	0.09	0.14	0.83	1.12	4.29	3.27	28.7	9.2	13.6	5.30
9	12.0	71	26	0.05	0.05	3.20	2.63	7.82	5.50	3.2	2.2	9.9	3.46
10	12.0	73	27	0.04	0.05	2.51	3.34	7.71	5.39	121.1	1.9	9.8	3.46
11	12.0	73	27	0.04	0.05	3.15	2.81	7.77	5.44	5.6	2.4	10.0	3.47
12	12.0	73	27	0.04	0.05	3.05	5.07	8.12	5.73	20.6	1.4	9.7	3.24
13	≈ 4												
14	12.0	63	24	0.04	0.05	3.05	2.24	7.54	5.25	14.0	2.4	9.2	3.23
15	12.0	77	28	0.04	0.11	0.36	0.22	4.98	2.47	275.1	126.6	14.2	6.08
16	12.0	76	27	0.05	0.07	2.00	1.42	5.71	3.48	8.3	7.6	11.7	4.38
17	12.0	70	26	0.05	0.05	3.09	3.73	8.20	5.90	9.1	1.3	9.7	3.30
18	12.0	69	23	0.08	0.13	0.32	0.22	4.56	2.17	371.1	121.3	14.9	6.41
19	12.0	69	24	0.09	0.12	1.41	1.12	5.00	2.90	68.7	122.9	12.1	4.64
20	12.0	30	14	0.05	0.14	0.20	0.17	3.05	1.30	678.2	126.0	12.0	4.92
21	12.0	66	25	0.04	0.12	0.37	0.05	4.54	2.02	226.6	2121.9	13.5	5.57
22	12.0	74	27	0.04	0.11	0.55	0.25	4.93	2.26	96.1	88.4	13.5	5.58
23	12.0	77	28	0.04	0.10	0.32	0.26	5.07	2.67	384.3	92.7	14.7	6.42
24	12.0	24	12	0.06	0.13	0.65	0.48	2.78	1.36	36.8	35.0	11.0	4.26
25	12.0	63	24	0.05	0.07	1.70	1.28	4.91	2.75	4.4	8.2	11.7	4.35
26	12.0	73	26	0.05	0.07	2.06	1.74	5.67	3.31	3.9	5.2	11.5	4.19
27	12.0	12	6	0.07	0.12	0.77	1.11	2.82	1.87	79.3	5.3	7.7	2.79
28	12.0	53	21	0.05	0.06	2.45	2.06	6.27	4.19	17.0	2.9	9.5	3.32
29	12.0	67	24	0.05	0.06	2.80	3.99	7.36	5.06	15.5	1.5	9.7	3.30
30	12.0	73	27	0.05	0.05	3.30	2.28	8.63	6.26	5.0	2.4	9.8	3.45
31	12.0	28	13	0.05	0.12	0.18	0.14	2.77	1.52	1124.2	205.1	13.7	5.78
32	12.0	20	10	0.06	0.09	1.02	1.44	2.89	1.92	13.9	8.1	9.7	3.39
33	≈ 4												
34	12.0	77	28	0.04	0.09	0.59	0.31	5.08	2.63	68.2	66.2	13.4	5.61
35	12.0	76	28	0.04	0.06	2.22	1.39	6.00	3.74	3.2	7.9	11.4	4.25
36	12.0	73	27	0.04	0.05	3.09	2.26	7.85	5.45	7.3	2.9	10.0	3.53
37	12.0	78	28	0.04	0.09	0.71	0.36	5.18	2.66	42.6	58.2	13.1	5.42
38	12.0	76	28	0.04	0.06	2.45	1.89	6.47	4.20	6.7	4.4	11.0	4.00
39	12.0	26	12	0.05	0.13	0.20	0.31	2.73	1.53	616.9	55.7	12.4	5.01
40	12.0	71	26	0.04	0.09	0.68	0.59	4.87	2.55	58.7	26.9	13.1	5.31
41	12.0	7	4	0.07	0.09	0.92	0.73	2.48	1.78	10.8	6.4	7.0	2.49
42	12.0	69	26	0.04	0.06	2.23	1.20	5.85	3.76	8.3	8.4	11.0	4.05
43	12.0	71	25	0.04	0.09	0.29	0.13	4.28	1.68	384.7	335.5	15.4	6.67
44	≈ 2												
45	12.0	74	25	0.04	0.07	0.21	0.18	4.63	2.06	966.6	175.1	13.5	5.85
46	12.0	72	25	0.04	0.08	0.20	0.14	4.46	1.97	1107.9	260.7	13.8	5.93
47	12.0	71	25	0.04	0.10	0.36	0.10	4.14	1.61	286.1	646.3	15.7	6.83
48	< 0.1												
49	≈ 3												
50	≈ 2												
51	12.0	69	25	0.05	0.05	3.58	4.72	8.57	6.17	3.7	1.1	9.3	3.10
52	11.0	77	28	0.04	0.10	0.56	0.26	4.73	2.31	89.7	112.1	14.5	6.06
53	12.0	74	27	0.05	0.06	2.50	1.57	6.28	4.07	2.6	5.8	11.0	4.05
54	12.0	63	24	0.05	0.05	3.96	7.76	10.55	7.95	10.4	0.5	8.2	2.58
55	12.0	69	26	0.04	0.05	3.64	2.20	8.38	5.90	2.4	2.4	9.4	3.31
56	12.0	77	28	0.04	0.09	0.76	0.56	5.09	2.61	34.4	35.1	13.3	5.49
57	≈ 0.6												
58	12.0	60	24	0.04	0.04	13.95	35.76	21.29	16.29	0.0	0.1	4.8	1.34
59	≈ 0.4												
60	12.0	67	23	0.09	0.12	1.86	1.16	5.33	3.15	5.7	10.7	11.4	4.36
61	12.0	64	22	0.09	0.13	0.36	0.14	3.56	1.61	647.6	9.2	17.0	7.27
62	12.0	65	23	0.09	0.11	2.42	1.46	6.50	4.24	5.7	253.7	10.3	3.79

NOTE. — Serial numbers for models are the same as in Table 1. Observed structural properties are denoted by the subscript “obs.” Definitions for observed properties are explained in §3. The approximate dissolution times (§3.2) are listed for dissolved clusters.

TABLE 3
PROPERTIES OF BLACK HOLES.

No.	N_{BH}	$N_{\text{BH,esc}}$	$N_{\text{BH-BH}}$	$N_{\text{BH-BH,esc}}$	$N_{\text{BH-nBH}}$	$N_{\text{BH-nBH,esc}}$	N_{merge}				M_{tot}	
							$z < 1$		$z < 2$		$z < 1$	
							in	out	in	out	(M_{\odot})	
1	464	1260	4	130	2	5	0	32	0	63	33.2	47.6
2	601	1001	2	97	1	2	0	17	0	46	34.7	46.7
3	165	1259	4	65	10	5	0	37	0	59	19.8	21.0
4	327	1213	4	132	2	1	0	42	0	83	26.7	30.5
5	393	1227	3	131	1	3	0	40	0	77	30.7	37.4
6	579	1200	4	146	1	6	0	45	0	80	32.0	44.9
7	139	1318	4	65	4	0	0	22	0	46	29.4	37.2
8	49	1458	6	103	4	11	0	32	0	55	21.6	39.0
9	458	1265	5	130	4	2	0	35	0	66	32.9	46.9
10	467	1286	3	156	1	37	0	39	0	68	35.4	43.3
11	437	1298	4	153	1	29	0	32	0	64	35.8	47.8
12	503	1367	2	159	2	23	0	42	0	66	35.7	50.8
13	686	1083	3	116	3	30	0	21	0	56	38.2	47.1
14	462	1346	3	151	4	32	0	44	0	75	32.1	50.9
15	6	1757	1	1	2	3	0	0	0	0	0.0	0.0
16	241	1465	3	89	2	0	0	25	0	49	28.1	45.6
17	759	967	3	138	5	2	0	50	0	71	34.9	49.5
18	1	1521	0	0	1	1	1	0	1	0	26.9	26.9
19	282	1218	4	172	6	11	0	52	0	102	19.6	28.6
20	0	1512	0	2	0	3	0	0	0	0	0.0	0.0
21	3	1637	1	0	0	2	1	0	1	0	11.6	11.6
22	3	1689	1	2	0	7	0	0	0	0	0.0	0.0
23	3	1797	0	2	1	7	1	0	1	0	37.5	37.5
24	132	1219	2	69	9	6	0	41	0	62	16.1	21.0
25	179	1345	2	80	3	2	0	25	0	54	25.6	30.7
26	239	1358	5	75	1	3	0	27	0	49	27.5	37.4
27	398	980	4	141	3	4	0	75	0	118	16.0	20.3
28	561	972	4	141	3	1	0	53	0	89	26.7	31.4
29	661	944	2	130	3	1	0	48	0	79	29.0	30.0
30	741	1046	7	145	1	5	0	43	0	76	30.3	48.0
31	1	1752	0	2	1	6	0	0	0	0	0.0	0.0
32	125	1418	3	81	1	4	0	36	0	51	27.9	48.0
33	881	671	3	94	3	1	0	20	0	51	36.2	45.0
34	18	1732	2	20	5	41	0	3	0	3	23.3	35.9
35	279	1432	3	158	6	17	0	17	0	37	30.0	44.1
36	673	1020	3	190	3	13	0	46	1	74	36.3	50.9
37	31	1794	2	25	4	52	0	5	0	5	22.9	26.3
38	338	1498	3	215	3	18	0	32	1	55	29.7	40.3
39	13	1723	0	30	5	57	0	7	0	7	19.6	21.9
40	31	1795	3	28	5	61	0	3	0	3	23.7	23.6
41	176	1422	2	214	0	17	0	26	2	49	26.9	43.2
42	315	1449	5	208	6	14	0	34	0	65	25.4	49.3
43	1	165	0	13	1	2	0	2	0	4	25.9	28.3
44	1430	5377	2	185	5	25	0	38	0	105	50.0	53.3
45	0	169	0	0	0	1	0	0	0	0	0.0	0.0
46	0	165	0	9	0	2	1	1	1	5	26.0	29.9
47	4	164	1	24	0	3	0	4	0	12	19.1	24.7
48	61	19012	0	30	0	45	0	0	0	0	0.0	0.0
49	1452	7774	5	148	4	10	1	48	1	78	49.2	53.8
50	1557	2502	4	202	4	9	0	38	0	106	49.9	54.4
51	393	1341	2	139	3	10	0	36	0	69	44.3	55.0
52	1	1764	0	1	1	12	0	0	0	0	0.0	0.0
53	165	1563	3	103	1	3	0	29	0	52	43.1	52.0
54	653	1068	1	162	2	2	0	31	0	59	49.7	57.2
55	310	1761	3	282	3	103	0	24	0	55	48.0	56.4
56	21	1916	1	51	5	160	0	1	0	2	60.2	60.2
57	1500	8638	9	248	2	75	0	28	1	94	54.6	56.4
58	39	19134	0	43	17	143	0	0	0	0	0.0	0.0
59	1917	3554	11	322	4	13	0	14	0	117	77.4	82.0
60	54	1469	1	141	3	7	0	33	0	59	33.6	43.7
61	1	1519	0	1	1	25	3	0	3	1	68.3	74.6
62	289	1237	3	175	7	10	0	31	0	69	34.3	43.0

NOTE. — Serial numbers for models are the same as in Table 1. Columns “in” and “out” denote BH-BH mergers inside and outside clusters. Number of BH-BH mergers and their total masses in the source frame are listed for $z < 1$ and $z < 2$ assuming $z = 0 \equiv t = 12$ Gyr. The median and 2σ ranges in total mass are listed.

- Pooley, D., Lewin, W. H. G., Anderson, S. F., Baumgardt, H., Filippenko, A. V., Gaensler, B. M., Homer, L., Hut, P., Kaspi, V. M., Makino, J., Margon, B., McMillan, S., Portegies Zwart, S., van der Klis, M., & Verbunt, F. 2003, *ApJ*, 591, L131
- Porras, A., Christopher, M., Allen, L., Di Francesco, J., Megeath, S. T., & Myers, P. C. 2003, *AJ*, 126, 1916
- Portegies Zwart, S. F. & McMillan, S. L. W. 2000, *ApJ*, 528, L17
- Portegies Zwart, S. F., McMillan, S. L. W., & Gieles, M. 2010, *ARA&A*, 48, 431
- Repetto, S., Davies, M. B., & Sigurdsson, S. 2012, *MNRAS*, 425, 2799
- Repetto, S. & Nelemans, G. 2015, *MNRAS*, 453, 3341
- Rodriguez, C. L., Morscher, M., Pattabiraman, B., Chatterjee, S., Haster, C.-J., & Rasio, F. A. 2015, *Physical Review Letters*, 115, 051101
- Rodriguez, C. L., Chatterjee, S., & Rasio, F. A. 2016a, *arXiv:1602.02444*
- Rodriguez, C. L., Morscher, M., Wang, L., Chatterjee, S., Rasio, F. A., & Spurzem, R. 2016b, *arXiv:1601.04227*
- Sana, H., de Mink, S. E., de Koter, A., Langer, N., Evans, C. J., Gieles, M., Gosset, E., Izzard, R. G., Le Bouquin, J.-B., & Schneider, F. R. N. 2012, *Science*, 337, 444
- Sigurdsson, S. & Hernquist, L. 1993, *Nature*, 364, 423
- Spera, M., Mapelli, M., & Bressan, A. 2015, *MNRAS*, 451, 4086
- Spitzer, Jr., L. 1969, *ApJ*, 158, L139
- Strader, J. 2014, A Black Hole in the Galactic Globular Cluster M10, Chandra Proposal
- Strader, J., Chomiuk, L., Maccarone, T. J., Miller-Jones, J. C. A., & Seth, A. C. 2012, *Nature*, 490, 71
- Strader, J., Miller-Jones, J., Maccarone, T., & Chomiuk, L. 2013, The ATCA Survey for Black Holes in Southern Globular Clusters, ATNF Proposal
- Umbreit, S. 2012, *Nature*, 490, 46
- Umbreit, S., Fregeau, J. M., Chatterjee, S., & Rasio, F. A. 2012, *ApJ*, 750, 31
- Van Eck, S., Jorissen, A., Udry, S., Mayor, M., & Pernier, B. 1998, *A&A*, 329, 971
- van Zyl, L., Charles, P. A., Arribas, S., Naylor, T., Mediavilla, E., & Hellier, C. 2004, *MNRAS*, 350, 649
- Vink, J. S. 2008, *New Astronomy Reviews*, 52, 419
- Vink, J. S., de Koter, A., & Lamers, H. J. G. L. M. 2001, *A&A*, 369, 574
- Wang, C., Lai, D., & Han, J. L. 2006, *ApJ*, 639, 1007
- Willems, B., Henninger, M., Levin, T., Ivanova, N., Kalogera, V., McGhee, K., Timmes, F. X., & Fryer, C. L. 2005, *ApJ*, 625, 324
- Wong, T.-W., Valsecchi, F., Ansari, A., Fragos, T., Glebbeek, E., Kalogera, V., & McClintock, J. 2014, *ApJ*, 790, 119
- Wong, T.-W., Valsecchi, F., Fragos, T., & Kalogera, V. 2012, *ApJ*, 747, 111
- Ziosi, B. M., Mapelli, M., Branchesi, M., & Tormen, G. 2014, *MNRAS*, 441, 3703
- Zuo, Z.-Y. 2015, *A&A*, 573, A58